MOLECULAR AND CELLULAR BIOLOGY, Sept. 2007, p. 5968–5985 Vol. 27, No. 17
0270-7306/07/$08.00+0 doi:10.1128/MCB.00019-07

Ribosomal Protein L33 Is Required for Ribosome Biogenesis, Subunit Joining, and Repression of *GCN4* Translation▽†

Pilar Martín-Marcos,[1] Alan G. Hinnebusch,[2] and Mercedes Tamame[1]*

Instituto de Microbiología Bioquímica, CSIC/Universidad de Salamanca, Edificio Departamental de Biología, Campus Miguel de Unamuno, 37007 Salamanca, Spain,[1] and Laboratory of Gene Regulation and Development, National Institute of Child Health and Human Development, Bethesda, Maryland 20892[2]

Received 4 January 2007/Returned for modification 8 February 2007/Accepted 21 May 2007

We identified a mutation in the 60S ribosomal protein L33A (*rpl33a-G76R*) that elicits derepression of *GCN4* translation (Gcd⁻ phenotype) by allowing scanning preinitiation complexes to bypass inhibitory upstream open reading frame 4 (uORF4) independently of prior uORF1 translation and reinitiation. At 37°C, *rpl33a-G76R* confers defects in 60S biogenesis comparable to those produced by the deletion of *RPL33A* (Δ*A*). At 28°C, however, the 60S biogenesis defect is less severe in *rpl33a-G76R* than in Δ*A* cells, yet *rpl33a-G76R* confers greater derepression of *GCN4* and a larger reduction in general translation. Hence, it appears that *rpl33a-G76R* has a stronger effect on ribosomal-subunit joining than does a comparable reduction of wild-type 60S levels conferred by Δ*A*. We suggest that *rpl33a-G76R* alters the 60S subunit in a way that impedes ribosomal-subunit joining and thereby allows 48S rRNA complexes to abort initiation at uORF4, resume scanning, and initiate downstream at *GCN4*. Because overexpressing $tRNA_i^{Met}$ suppresses the Gcd⁻ phenotype of *rpl33a-G76R* cells, dissociation of $tRNA_i^{Met}$ from the 40S subunit may be responsible for abortive initiation at uORF4 in this mutant. We further demonstrate that *rpl33a-G76R* impairs the efficient processing of 35S and 27S pre-rRNAs and reduces the accumulation of all four mature rRNAs, indicating an important role for L33 in the biogenesis of both ribosomal subunits.

Cell growth and division are highly interconnected processes that require protein synthesis, which in turns requires the biogenesis of ribosomes, soluble translation factors, and charged tRNA species. In *Saccharomyces cerevisiae*, ribosome biogenesis consumes a great amount of energy and is tightly regulated according to nutrient availability and to signals depending on other macromolecular pathways (77). The production of 60S and 40S ribosomal subunits is a highly dynamic process that begins with the transcription of rRNA by RNA polymerase I (35S rRNA precursor to 25S, 18S, and 5.8S rRNAs) and RNA polymerase III (5S rRNA) in the nucleolus and ends with export of preribosomal 60S and 40S subunits to the cytoplasm, where final steps of maturation occur. The maturation pathway of the 35S pre-rRNA to yield 25S, 18S, and 5.8S rRNAs (see Fig. 4A) is closely coordinated with the assembly of 79 ribosomal proteins (r-proteins) and more than 150 *trans*-acting factors involved in the synthesis, maturation, and transport of the ribosomal subunits (reviewed in references 11, 41, 53, and 73). The association of 35S pre-rRNA with the U3-snoRNP complex, transiently associated *trans*-acting factors, and several r-proteins, mostly belonging to the 40S subunit, leads to the formation of the 90S nucleolar complexes, where cleavage at the A0, A1, and A2 processing sites occurs (16, 28; reviewed in reference 29). The pre-40S particle, which contains some newly associated maturation factors and some already present in the 90S particle, is released after A0-A1-A2 cleavage and transported to the cytoplasm, where cleavage of 20S pre-rRNA to mature 18S rRNA occurs (59). Independently, several pre-60S particles are assembled that differ in the compositions of their rRNAs (distinct 27S precursors) and *trans*-acting factors, which are mostly are not found in the 90S particle (4, 20, 33, 51, 58).

In *S. cerevisiae*, genetic analysis and recent biochemical approaches have shed light on the sequence of incorporation of assembly factors into preribosomal 60S and 40S particles during assembly and export (reviewed in references 47 and 67). In contrast, much less is known about the contribution of r-proteins to ribosome biogenesis, because they were found as contaminants in most protein complexes identified in comprehensive analyses of protein-protein interactions in yeast (25). Thus, it was impossible to faithfully determine their precise sequential assembly with the early 90S particle, or with 40S and 60S preribosomes (16, 28, 29, 51). However, it is well documented that insufficiency of a single r-protein often leads to aberrant processing of pre-rRNAs and to insufficient production of mature ribosomal subunits. A recent systematic study in yeast revealed that most of the 32 r-proteins of the small 40S subunit (rpS proteins) play roles in ribosome biogenesis and are essential for growth (22). Distinct rpS proteins are required for early and/or late maturation steps of the 20S pre-rRNA to 18S rRNA or for intracellular transport of the small subunit, suggesting that their correct assembly would guarantee the production of 40S particles fully functional in translation. Although a similar systematic analysis of the 46 r-proteins of the yeast 60S subunit (rpL proteins) has not yet been reported, experimental evidence that rpL proteins are also required for pre-rRNA processing exists. Thus, the absence or functional

* Corresponding author. Mailing address: Mercedes Tamame, Instituto de Microbiología Bioquímica, CSIC/Universidad de Salamanca, Edificio Departamental de Biología, Campus Miguel de Unamuno, 37007 Salamanca, Spain. Phone: 34 923 121673. Fax: 34 923 224876. E-mail: tamame@usal.es.

† Supplemental material for this article may be found at http://mcb.asm.org/.

▽ Published ahead of print on 4 June 2007.

inactivation of rpL5, rpL11, rpL25, rpL28, or rpL30 affects pre-rRNA processing, resulting in similar phenotypes of accumulation of 35S and 27S pre-rRNA species suggestive of delayed processing at A0, A1, and A2 and of the late cleavage step at C2 (12, 48, 70, 72, 74).

Several r-proteins have been shown to mediate interactions with specific *trans*-acting factors required for the maturation of pre-rRNAs and ribosomal assembly, while others interact with components of the translation machinery (translation factors or tRNAs), and some are required for the efficient execution of the early or late steps of the translation process. For instance, (i) the physical interaction of rpS14 with the FAP7 assembly factor is required for the cleavage of the 20S pre-rRNA in pre-40S particles (30); (ii) the interaction of rpS0 with the TIF32 subunit of the translation initiation factor eIF3 may mediate eIF3 recruitment to mature 40S subunits (71); (iii) rpL5 helps to anchor the peptidyl-tRNA to the "P" site of the ribosome (45); (iv) the lack of any of the nonessential r-proteins rpL41, rpL24, and rpL39 or mutant forms of essential rpL3 affect the peptidyl-transferase activity of the resulting ribosomes (17, 18, 19, 46); and (v) the nascent polypeptide-associated factor gains access to nascent polypeptides via its interaction with rpL25 at the exit site of the ribosome (27).

Mutations that disrupt the translational regulation of the distinctive *GCN4* mRNA in *S. cerevisiae* have identified essential components of the translational apparatus, including initiation factors that control initiator $tRNA_i^{Met}$ binding to the 40S ribosome and r-proteins (37, 38). GCN4 is one of the best-characterized transcriptional activators, first identified by its role in a major physiological response known as the general amino acid control (GAAC) response. The sophisticated mechanism that couples *GCN4* expression to amino acid availability has been explored in great detail (see reference 38 for a review) and depends on four short, upstream open reading frames (uORFs) located in the *GCN4* mRNA leader and on multiple *trans*-acting factors encoded by the *GCN* and *GCD* genes. Under conditions of amino acid sufficiency, the four uORFs prevent ribosomes from initiating translation at the *GCN4* start codon, and very little GCN4 protein is produced. However, whereas solitary uORF1 reduces *GCN4* expression by ~50%, uORF3 and -4 are the critical negative elements in the leader, and ribosomes that translate these sequences cannot reinitiate at the AUG codon of *GCN4*. Under amino acid starvation conditions, uORF1 has a stimulatory role, allowing ribosomes to traverse inhibitory uORF3 and -4 without initiating translation and reinitiate at GCN4 instead. This up-regulation occurs because uncharged tRNA species that accumulate in amino acid-starved cells activate the protein kinase GCN2, which phosphorylates the α-subunit of translation initiation factor 2 (eIF2). This modification reduces the rates of general protein synthesis, because it inhibits the delivery of charged methionyl initiator tRNA to the 40S ribosomal subunit by the eIF2 · GTP · $tRNA_i^{Met}$ ternary complex (TC). In contrast, the delayed recruitment of the TC enables 40S subunits that have translated uORF1 and resumed scanning to bypass inhibitory uORF3 and -4 and eventually initiate at the GCN4 start codon downstream. Thus, contrary to most mRNAs, *GCN4* translation is induced by a decreased availability of the TC in cells (15). However, induction of *GCN4* occurs at a lower level of eIF2α phosphorylation than is required for general inhibition of protein synthesis, making it a sensitive reporter of decreased TC formation and of defects in TC recruitment to the 40S ribosome (14).

The GCD factors are required for the repression of *GCN4* mRNA translation under conditions of amino acid sufficiency. The *GCD* genes were identified by recessive mutations that constitutively derepress *GCN4* translation in the absence, or reduced function, of the eIF2α kinase GCN2 (10, 32). All known GCD proteins have functions in the initiation of protein synthesis or regulate the activities of initiation factors and are essential for growth. Consistently, all Gcd^- mutants analyzed so far display slow-growth phenotypes at 28°C (Slg^-) that are more noticeable at the higher temperatures of 34°C and 37°C. Here we have identified a new complementation group of Gcd^- mutants defined by the *gcd17-1* mutation. The *GCD17* gene was cloned and shown to be identical to *RPL33A*, one of the two genes encoding the essential r-protein L33 in yeast (65), which belongs to a conserved family of proteins that bind tRNA. The *gcd17-1* mutation, which replaces Gly-76 with Arg in rpL33A, impairs efficient early processing of 35S and 27S pre-rRNAs and greatly impedes the accumulation of 60S ribosomal subunits at the restrictive growth temperature of 37°C. This leads to the formation of half-mer polysomes, indicating a decreased rate of 60S subunit-to-40S subunit joining at the final step of translation initiation and a strong reduction in the rate of general protein synthesis. Interestingly, at 28°C, *rpl33a-G76R* constitutively derepresses *GCN4* translation, producing a Gcd^- phenotype that is considerably stronger than that produced by the null, deletion allele of *RPL33A* (strain Hm506 [Δ*A* mutation]). This is remarkable because *rpl33a-G76R* is less severe than Δ*A* in reducing 60S subunit levels at this growth temperature. Analysis of *GCN4-lacZ* reporters suggests that both *rpl33a-G76R* and Δ*A* mutations derepress *GCN4* translation in the presence of high TC levels (i.e., in the *gcn2* background) by impairing 60S-40S subunit joining at uORF4 of the *GCN4* mRNA leader. Thus, *rpl33a-G76R* might impede the joining reaction and efficient 80S initiation complex formation. We propose that inefficient subunit joining at uORF4 allows 40S subunits to abort initiation at the uORF4 start site, resume scanning, and reinitiate downstream at *GCN4.* Our finding that the Gcd^- phenotype of the *rpl33a-G76R* mutation is suppressed by overexpressing $tRNA_i^{Met}$ suggests that the dissociation of $tRNA_i^{Met}$ from the 40S subunit is responsible for the postulated abortive initiation events at uORF4. Thus, our data indicate that rpL33 has a critical function in the ribosome biogenesis pathway required for the efficient production of both ribosomal subunits and a second role in translation initiation at the stage of 40S subunit-60S subunit joining. Both activities contribute to the repression of *GCN4* translation under nonstarvation conditions and, hence, the proper functioning of the GAAC response.

MATERIALS AND METHODS

Plasmids. (i) Cloning of *GCD17* and *gcd17-1* alleles. Plasmid pPM1, bearing an ~11-kb DNA fragment of yeast chromosome XVI, was isolated from a yeast genomic library in YCp50 (55). Subclones of the genomic insert in pPM1 were constructed in the shuttle vector pRS316 in order to define the boundaries of *GCD17*. Plasmid pPM2 bears a 1.9-kb SalI-NdeI genomic fragment from pPM1 cloned in pRS316, containing YPL143W (*RPL33A*) and the dubious ORF YPL142C encoded in the Crick strand, in the opposite orientation relative to YPL143W. Plasmid pPM26 bears an 882-bp HindIII-NdeI fragment with

TABLE 1. Yeast strains

Strain	Genotype	Reference or source
H96	*MAT*α *gcn2-101 gcn3-101 his1-29 ura3-52* (*HIS4*::*lacZ ura3-52*)	32
H117	*MAT***a** *gcn2-101 gcn3-101 his1-29 ino1 ura3-52* (*HIS4*::*lacZ URA3*)	32
H275	*MAT***a** *gcn2-101 gcn3-101 his1-29 ino1 ura3-52* (*HIS4*::*lacZ URA3*) *rpl33a-G76R*	10
Hm337	*MAT*α *gcn2-101 gcn3-101 his1-29 ino1 ura3-52* (*HIS4*::*lacZ ura3-52*) *rpl33a-G76R*	H275 × H96
Hm506	*MAT***a** *gcn2-101 gcn3-101 his1-29 ino1 ura3-52* (*HIS4*::*lacZ ura3*) *rpl33a*::*URA3*	This study
Hm502	*MAT***a** *gcn2-101 gcn3-101 his1-29 ino1 ura3-52* (*HIS4*::*lacZ URA3*) *rpl33b*::*kanMX4*	This study
Hm505	*MAT***a** *gcn2-101 gcn3-101 his1-29 ino1 ura3-52* (*HIS4*::*lacZ URA3*) *rpl33a-G76R rpl33b*::*kanMX4*	This study
Hm525	*MAT***a** *gcn2-101 gcn3-101 his1-29 ino1 ura3-52* (*HIS4*::*lacZ URA3*) *rpl33a*::*kanMX4*	This study
H466	*MAT*α *gcn2-101 gcn3-101 ura3-52*	32
Hm526	*MAT*α *gcn2-101 gcn3-101 ura3-52 rpl33a*::*kanMX4*	This study
Hm527	*MAT*α *gcn2-101 gcn3-101 ura3-52* (*rpl33a-G76R kanMX4*::*rpl33a*)	This study
S288C	*MAT*α *SUC2 gal2 mal mel flo1 flo8-1 hap1*	ATCC 204508
F35	*MAT***a** *ura3-52 ino1 can1* (*HIS4*::*lacZ URA3*)	43
Hm531	*MAT***a** *ura3-52 ino1 can1* (*HIS4*::*lacZ URA3*) *rpl33a*::*kanMX4*	This study
Hm532	*MAT***a** *ura3-52 ino1 can1* (*HIS4*::*lacZ URA3*) (*rpl33a-G76R-kanMX4*::*rpl33a*)	This study
JWY2165	*MAT***a** *ura 3-52 his3-11,15 leu2-3,112 drs1-1*	54
JWY6882	*MAT*α *his3*Δ*-200 leu2-*Δ*1 lys2-801 trp1-*Δ*101 ura3-52 nop7*::*HIS3* plus pNOP7A (CEN *LEU2 nop7-A*)	J. L. Woolford

YPL142C cloned in pRS316 and does not complement the phenotypes of *gcd17-1*. Plasmid pPM13 was constructed by cloning a 1.9-kb SalI-XbaI fragment containing *RPL33A* in pRS426 (hc*RPL33A*). The *gcd17-1*/*rpl33a-G76R* mutation was identified by independent PCR amplification of the corresponding mutant allele from genomic DNAs of strains H275 and Hm337 (Table 1), with oligonucleotides F4 (5′-CGCATAACTCTTCGATAATACAG-3′) and R5 (5′-CCAAA GTCCAGAACATTCAACC-3′) used as primers, followed by automatic sequencing of the amplification products on the two DNA strands.

(ii) Construction of *rpl33a* and *rpl33b* null alleles. Plasmid pPM18 was constructed as follows: the 1.9-kb XbaI-SalI fragment of chromosome XVI containing YPL143W (*RPL33A*), including 610 bp upstream of the ATG start codon and 493 bp downstream of the stop codon, was cloned in pRS315. A 519-bp HindIII fragment internal to the *RPL33A* ORF was replaced with a 1.1-kb fragment containing the *URA3* gene. The 2.5-kb null allele *rpl33a*::*URA3* is excised from pPM18 by digestion with SalI and XbaI.

The null allele *rpl33a*::*kanMX4* was constructed by PCR-long flanking homology analysis (75). In a first PCR, plasmid pPM2 (see above) was used as the template to amplify a 164-bp sequence of the *RPL33A* coding region, using primers L1A and L2A, and a 601-bp sequence corresponding to the 3′ region of *RPL33A*, using primers L3A and L4A. To construct the *rpl33b*::*kanMX4* null allele of *RPL33B*, plasmid pPM10 bearing a 3.1-kb SalI-SalI fragment of chromosome XV containing *RPL33B*, was used as the template to amplify by PCR (i) a 429-bp sequence of the *RPL33B* 5′ region, using primers L3B and L4B, and (ii) a 614-bp sequence corresponding to the 3′ region downstream of the *RPL33B* stop codon, using primers L1B and L2B. L1A is 5′CTTCTACTCTTCACCGG CATG3′), L2A is 5′GGGGATCCGTCGACCTGCAGCGTACCATTTTTCAA TTTATTTGATTGTTGG3′, L3A is 5′AACGAGCTCGAATTCATCGATGAT ATGACGCATAACTCTTCGATAATACAG-3′, L4A is 5′-GCTTACAGCGA GATTCGCAG-3′, L1B is 5′CTCAGCAGCAACCACGTAAC-3′, L2B is 5′GG GGATCCGTCGACCTGCAGCGTACCATGACTTTCGGTGCCTCTG TCAG3′, L3B is 5′AACGAGCTCGAATTCATCGATGATATGAATACGTC TATGGGATTCAGC3′, and L4B is 5′GAAACGTACGGTATATTGTGAG-3′. Primers L2 and L3 carry 28-nt 5′ extensions (underlined) complementary to the *kanMX4* module cloned into the pFA6a-KanMX4 plasmid (76), which was used as the template to amplify the *kanMX4* sequences in a second PCR, using as primers the 164-bp and 601-bp fragments (*RPL33A*) or 614-bp and 429-bp fragments (*RPL33B*) amplified before. These reactions produce a 2.3-kb fragment containing an *rpl33a*::*kanMX4* null allele and a 2.5-kb fragment containing an *rpl33b*::*kanMX4* null allele, respectively.

Plasmids pJW6039 (hc*NOP7*) and pJW3015 (hc*DRS1*) were kindly provided by J. W. Woolford, Jr. (Carnegie Mellon University, Pittsburgh, PA). Plasmid p2635 (hc*IMT4*) was previously described (2). Plasmid p1730-*IMT4* (p3000) contains the *SUI2*, *SUI3*, and *GCD11* genes, encoding, respectively, the α, β, and γ subunits of yeast eIF2, and the *IMT4* gene, all cloned in YEp24 (3). Plasmid pAS425 contains the *PAB1* gene cloned in a 2μm URA3 vector and was kindly provided by A. Sachs (University of California at Berkeley).

Yeast strain construction. The *Saccharomyces cerevisiae* strains used in this study are listed in Table 1. *RPL33A* and *RPL33B* were individually replaced with the null allele *rpl33a*::*URA3*, *rpl33a*::*kanMX4*, or *rpl33b*::*kanMX4* in the wild-type (WT) H117 strain. By contrast with the *rpl33a*::*LEU2* null allele (65), the *rpl33a*::*URA3* and *rpl33a*::*kanMX4* alleles were constructed to preserve the integrity of YPL142C, a hypothetical ORF located on the strand opposite to *RPL33A*, which was annotated as essential (SGD). To produce strain Hm506 (*rpl33a*::*URA3* [Δ*A*]), a Ura$^-$ spontaneous derivative of H117 (*URA3 HIS4*::*lacZ*) selected in 5-fluoroorotic acid was transformed with the SalI-XbaI fragment from pPM18 containing *rpl33a*::*URA3*. Correct replacement of *RPL33A* by *rpl33a*::*URA3* was verified by Southern blotting, with digestion of total DNA of the corresponding transformants with PstI and SalI and the use of sequences complementary to *URA3* and *RPL33A* as probes.

To produce strain Hm525, strain H117 (*URA3 HIS4*::*lacZ*) was transformed with a 2.3-kb fragment containing the *rpl33a*::*kanMX4* null allele described above. To produce strains Hm502 (*rpl33b*::*kanMX4* [Δ*B* mutation]) and Hm505 (*rpl33a-G76R*Δ*B*), the 2.5-kb null allele *rpl33B*::*kanMX4* was used to transform strains H117 (*RPL33A*) and H275 (*rpl33a-G76R*), respectively. Geneticin-resistant transformants were selected on yeast extract-peptone-dextrose (YPD) plates with 100 μg/ml of Geneticin (G-418), and in every case, correct replacements by the null alleles were verified by PCR using the appropriate oligonucleotides. To create Δ*A* and *rpl33a-G76R* mutations in a *gcn2-101 gcn3-101* background devoid of the integrated *HIS4-lacZ* fusion, the *RPL33A* gene was replaced in strain H466 with the *rpl33a*::*kanMX4* null allele (described above) or with a marked allele, *rpl33a-G76R-kanMX4*, generating the isogenic mutants Hm526 (*gcn2-101 gcn3-101 rpl33a*::*kanMX4*) and Hm527 (*gcn2-101 gcn3-101 rpl33a-G76R-kanMX4*), and correct replacements were verified by PCR. The *rpl33a-G76R-kanMX4* marked allele was constructed by inserting a fragment of 1.4 kb from plasmid pFA6a-KanMX4 (76) containing the *kanMX4* marker into the NdeI site located at the 3′ end of the functional *rpl33a-G76R* sequence, which was cloned as a SalI-XbaI fragment of 1.9 kb in plasmid pRS315 (pPM28). The marked allele *rpl33a-G76R-kanMX4* is excised from pPM28 as a 3.1-kb EcoRI-XbaI fragment. It contains the *rpl33a-G76R* ORF flanked by genomic sequences upstream (276 bp) and downstream (449 bp), followed by *kanMX4*.

Media. Yeast strains were grown in rich YPD medium or in standard dextrose (SD) medium supplemented as required. Starvation for histidine with 3-aminotriazol (3AT) or for tryptophan with 5-methyltryptophan (5MT) was tested as described previously (32, 39).

Biochemical techniques. (i) Assay of *HIS4-lacZ* and of *GCN4-lacZ* fusions. β-Galactosidase assays were conducted as previously described (7) with cells grown in SD medium containing only the required supplements to an optical density at 600 nm (OD_{600}) of ~1. For repressing conditions, cultures were harvested in mid-logarithmic phase after 8 h of growth. For derepressing conditions, cells were grown for 3 h under repressing conditions and then for 6 h after 3AT was added to 10 mM. The values shown in Table 3 and Fig. 5D are the averages of results from three independent determinations. β-Galactosidase activities are expressed as nanomoles of *o*-nitrophenyl-β-D-galactopyranoside cleaved per minute per ~1×10^7 cells.

(ii) Northern analysis. To measure the steady-state levels of pre-rRNA and rRNA in WT H117 and in the *rpl33a-G76R* mutant H275, Northern analysis was carried as follows. In all experiments, cells were grown in liquid YPD medium at 28°C to and OD_{600} of ~1 (time zero) and then transferred to 37°C for several

hours. Total RNA was extracted from equivalent numbers of cells (5×10^8) of these strains by the phenol-acid method (60). Samples containing 10 μg of total RNA were electrophoresed in 1.2% agarose–4% formaldehyde gels for analysis of rRNAs. The RNAs were blotted to positively charged nylon membranes (Roche) and immobilized by UV cross-linking with a UV Stratalinker 2400 (Stratagene). The blots were hybridized sequentially with ~20-nucleotide-long oligonucleotides labeled at their 5′ ends with [γ-^{32}P]ATP (6,000 Ci/mmol), and direct quantification of the corresponding hybridization signals was performed by PhosphorImaging analysis using MacBas-v2.5 and a BAS-1500 PhosphorImager. The oligonucleotides used as probes are listed below, and those designated 1 to 7 are complementary to rRNA sequences indicated in Fig. 4A. Oligonucleotide 1 is 5′TCAGGTCTCTCTGCTGC3′, 2 is 5′AGCCATTCGCAGTTTCACTG3′, 3 is 5′TTAAGCGCAGGCCCGGCTGG3′, 4 is 5′TGTTACCTCTGGGCCC3′, 5 is 5′TGCGTTCTTCATCGATGCGAGAACC3′, 6 is 5′GGCCAGCAATTTC AAGTTA3′, 7 is 5′TACTAAGGCAATCCGGTTGG3′, 8 (*5S*) is 5′CAGTTG ATCGGACGGGAAAC3′, 9 (*U3*) is 5′GGATTGCGGACCAAGCTAA3′, and 10 (*SCR1*) is 5′GAGGGAACGGCCACAATGTG3′. When mRNAs were analyzed, total yeast RNA was prepared and RNA blot hybridization was carried out as described previously (35). A 3.1-kb PCR product containing the entire *HIS4* gene sequence was used as the radiolabeled probe for *HIS4* mRNA, and a 6.7-kb HindIII fragment containing the entire pyruvate kinase-coding sequence (*PYK1*) was used as the probe for *PYK1* mRNA. A 450-bp KpnI-MluI fragment was used as the probe for *GCN4* mRNA, and a 601-bp PCR fragment corresponding to the 3′ end of the *RPL33A* gene was used as the probe for *RPL33A* and *RPL33B* mRNAs.

(iii) Polysome analysis. Polysome analysis by sucrose gradient centrifugation was basically done as previously described (23). Cells were grown in YPD at 28°C to mid-logarithmic phase, and then cultures were incubated at 37°C and an OD_{600} of ~1. When the cells were harvested, cycloheximide was added at a final concentration of 100 μg/ml. Whole-cell extracts (WCE) were extracted as described in reference 23 and loaded onto 7% to 50% gradients, which were scanned at 254 nm. For ribosomal-subunit quantification, low-Mg^{2+} sucrose gradients and WCE were prepared in the absence of cycloheximide.

(iv) Measurement of radioactive-methionine incorporation into protein. Radioactive-methionine incorporation was measured as described in reference 5, with some modifications. Cells were grown in 200 ml of SD medium containing the necessary supplements and lacking methionine at 28°C to an OD_{600} of ~0.6 and then transferred to 37°C for 3 or 6 h. Duplicate 1-ml aliquots were removed at the times indicated and incubated with 5 μCi of L-[^{35}S]methionine (>1,000 Ci/mmol; Amersham) and unlabeled methionine to a final concentration of 0.25 mM for 10 min at 28°C. Incorporation of the radiolabeled methionine was monitored by trichloroacetic acid (TCA) precipitation. TCA (3 ml of a 5% solution) was added to each aliquot, followed by heating at 90°C for 15 min and incubation on ice. The precipitates were collected on GF/C filters, which were washed three times with 10 ml of 5% TCA and 15 ml of 95% ethanol, and dried under a heat lamp, and cells were counted by scintillation spectrometry.

RESULTS

Phenotype of *gcd17* mutants. The Gcd$^-$ mutant H275 was isolated as a spontaneous suppressor of the Gcn$^-$ phenotype of the *gcn2-101 gcn3-101* strain H117 (10, 32). Further genetic analysis showed that H275 carries a monogenic *gcd* mutation, which confers a semidominant Gcd$^-$ phenotype in heterozygous *gcd*/*GCD* diploids (10). In this study, we found that H275 defines a new complementation group of Gcd$^-$ mutants, designated *gcd17* mutants. All *gcn2* and *gcn3* mutations confer sensitivity to 3AT, because they impair derepression of *GCN4* and of histidine biosynthetic genes regulated by GCN4 in response to histidine starvation imposed by 3AT (39). The *gcd17-1* mutation confers 3AT resistance in a *gcn2-101 gcn3-101* background (Fig. 1A), suggesting that it derepresses *GCN4* translation. In addition, H275 exhibits a severe Slg$^-$ phenotype on minimal media at 28°C, which is exacerbated at both higher (32°C to 37°C) and lower (13°C to 18°C) temperatures, such that very tiny colonies arise on plates of minimal medium only after incubation for 4 days (37°C) or 10 to 12 days (18°C) (Fig. 1B). Aberrant cell morphologies were also observed for H275 at restrictive and permissive temperatures (Fig. 1C). The Gcd$^-$ phenotype, slow growth, and cell morphology defects of the *gcd17* mutant suggest that, in addition to having a role in general amino acid control, the *GCD17* product has an essential function that indirectly affects cell cycle or morphogenetic events. In support of a possible role for GCD17 in translation, we found that H275 showed an increased sensitivity to drugs that affect protein synthesis (Fig. 1D).

Under amino acid starvation conditions, GCN4 activates the transcription of the *HIS4* gene and a large number of amino acid-biosynthetic genes (36). More recently, whole-genome studies have shown that GCN4 activates 77 amino acid-biosynthetic genes and directly or indirectly regulates a very large set of 539 genes, encompassing ~1/10 of the yeast genome (50). Gcd$^-$ mutants exhibit high levels of *HIS4* transcription under conditions of amino acid sufficiency owing to constitutive derepression of *GCN4* expression. Consistent with this, under amino acid-replete conditions, levels of β-galactosidase synthesized from a *HIS4-lacZ* fusion construct were fivefold higher in the *gcd17* mutant H275 than in the isogenic *GCD17* strain H117 (10). Here, we show that the *gcd17-1* mutation elicits high levels of *HIS4* mRNA in the *gcn2-101 gcn3-101* background both under nonstarvation conditions of growth in minimal medium (SD) and under tryptophan limitation imposed by 5MT (Fig. 1E). Relative to the levels of *PYK1* mRNA used as the internal control, the levels of *HIS4* mRNA were 5-fold higher in the *gcd17* mutant H275 than in the *GCD17* parent H117, while those of *GCN4* mRNA were only ~1.5-fold higher in the mutant. The WT *GCN GCD* strain F35 exhibits levels of *HIS4* mRNA ~11 times higher when it is grown in 5MT than when it is grown in SD medium (Fig. 1E). These data are consistent with the idea that *gcd17-1* leads to a partial derepression of *GCN4* translation, with attendant derepression of the GCN4 target gene *HIS4*.

Cloning of *GCD17* and of the *gcd17-1* mutant allele. The WT allele of *GCD17* was cloned in plasmid pPM1 from a yeast genomic library (Materials and Methods) by complementing the recessive Slg$^-$ phenotype at 34°C of the *gcd17-1 ura3-52* strain Hm337 (Table 1). Subcloning of the genomic insert contained in pPM1 and complementation analysis identified YPL143W, encoding the 60S ribosomal-subunit protein rpL33A (Materials and Methods). To distinguish between complementation by *GCD17* and dosage-dependent suppression of the *gcd17-1* mutation, an 882-bp HindIII-NdeI fragment of the pPM1 insert corresponding to the 3′ end of the *RPL33A* gene (http://db.yeastgenome.org/cgi-bin/locus.pl?locus=rpl33a) was subcloned into a nonreplicating *URA3* plasmid and shown to direct plasmid integration into the *gcd17* locus (*rpl33a*) in Hm337 (data not shown). As the integration event restored WT growth to Hm337, it verified by marker rescue that *RPL33A* is the WT allele of *GCD17* and mapped the *gcd17-1* mutation to the corresponding 882-bp HindIII-NdeI fragment of the *rpl33a* mutant allele.

rpL33A, previously designated L37 (or Rp47) in *S. cerevisiae* (44), is encoded by duplicate genes, *RPL33A* (XVI) and *RPL33B* (XV), which are differentially expressed. The *RPL33A* gene was estimated to produce mRNA levels sixfold higher than those generated from *RPL33B* when fused to a *LAC4* reporter gene. Accordingly, a null Δ*rpl33a*::*LEU2* mutant is viable but severely impaired in growth, and a Δ*rpl33b*::*URA3*

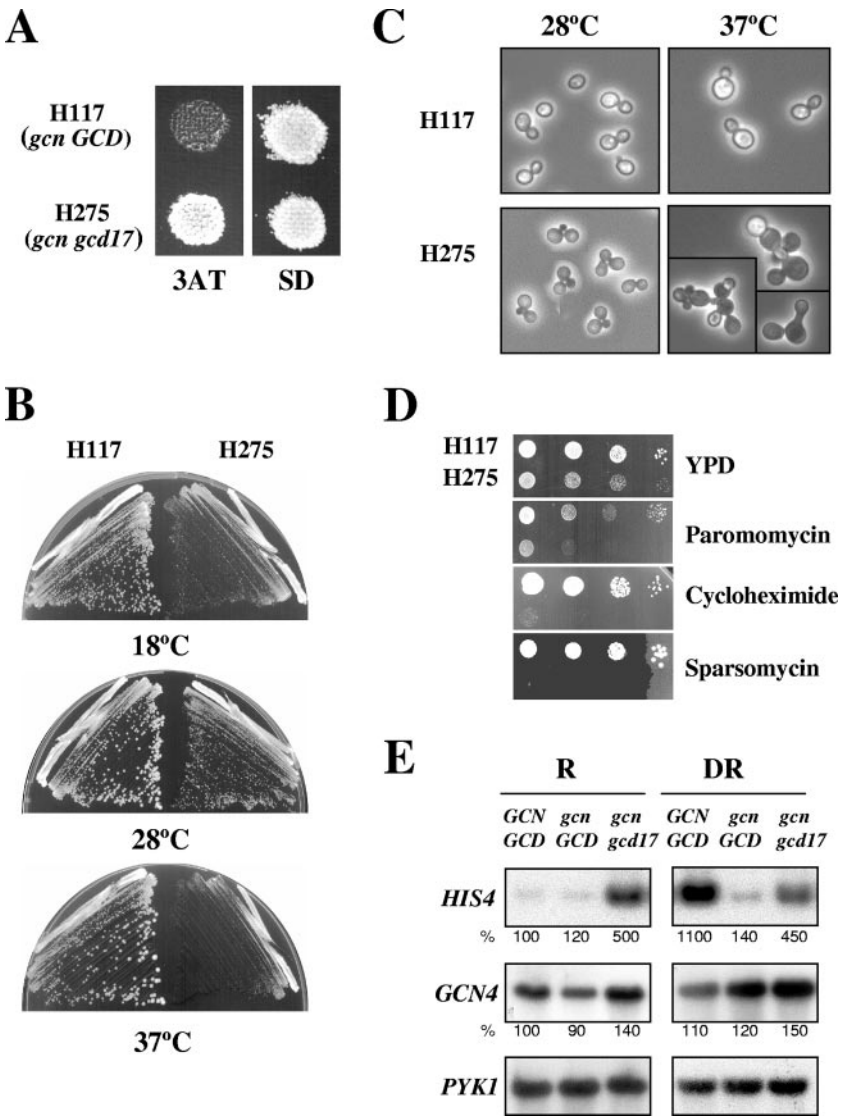

FIG. 1. Gcd$^-$ (3AT^R), Slg$^-$, cell morphology, and antibiotic-sensitivity phenotypes of the H275 mutant (*gcd17-1*/*rpl33a-G76R*). (A) 3AT^R phenotype of H275 relative to the 3AT^S phenotype of the isogenic WT *GCD17* strain H117 (*gcn2-101 gcn3-101*). Isolated colonies of each strain were replica printed to plates containing 10 mM 3AT and to minimally supplemented SD medium plates and incubated for 3 days at 28°C. (B) Slg$^-$ phenotype of H275 at 18°C, 28°C, and 37°C. Cells were streaked for single colonies on SD plates that were incubated at 18°C (10 days), 28°C (3 days), or 37°C (4 days). (C) Aberrant cell morphologies of the H275 mutant. Cells of H117 and of the H275 mutant were grown for 24 h in liquid YPD at 28°C or 37°C, and pictures were taken under a phase-contrast microscope (magnification, ×40). (D) Increased sensitivity of the H275 mutant to the protein synthesis inhibitors paromomycin (500 μg/ml), cycloheximide (0.025 μg/ml), and sparsomycin (5 μg/ml) relative to that of H117. Serial dilutions of cells (10^4 to 10 cells) grown for 12 h in YPD were plotted on YPD plates and on YPD plates containing the indicated concentrations of antibiotics and incubated for 3 or 4 days at 28°C. (E) The *gcd17-1*/*rpl33a-G76R* mutation increases the transcription of the *HIS4* gene. Cells of isogenic strains H117 (*gcn GCD17*) and H275 (*gcn gcd17-1*) and of the WT strain F35 (*GCN GCD*) were grown under repressing (R) (SD medium) and derepressing (DR) conditions of tryptophan starvation induced by 0.5 mM 5MT. Total RNA was extracted and 10 μg analyzed by Northern blot analysis in three independent blots, using radiolabeled probes specific to visualize *HIS4*, *GCN4*, and *PYK1* mRNAs (Materials and Methods). The hybridization signals were quantified by PhosphorImaging analysis, and values normalized relative to *PYK1* mRNA are given in percentages below each panel relative to the corresponding values in F35, which were set to 100%.

mutant exhibits normal growth, while Δ*rpl33a* Δ*rpl33b* double mutants are inviable, indicating that rpL33 is an essential protein (65). The coding region of *RPL33A* is very similar to that of *RPL33B*, with only one conservative amino acid difference (Asp-40 in rpL33A and Glu-40 in rpL33B); however, overexpression of either *RPL33A* or *RPL33B* complements the phenotypes of the deletion mutants, indicating that both products are functional (65). Recently, it was shown that rpL33A is haploinsufficient in rich medium (YPD), while the loss of rpL33B only slightly reduces fitness (13).

We determined that the *gcd17-1* mutation in mutants H275 and Hm337 is a single-point mutation (see Materials and Methods) consisting of a transversion from G to C at nucleotide 750 of the *RPL33A* ORF, replacing a glycine codon (GGT) with an arginine codon (CGT) at amino acid residue 76 of rpL33A.

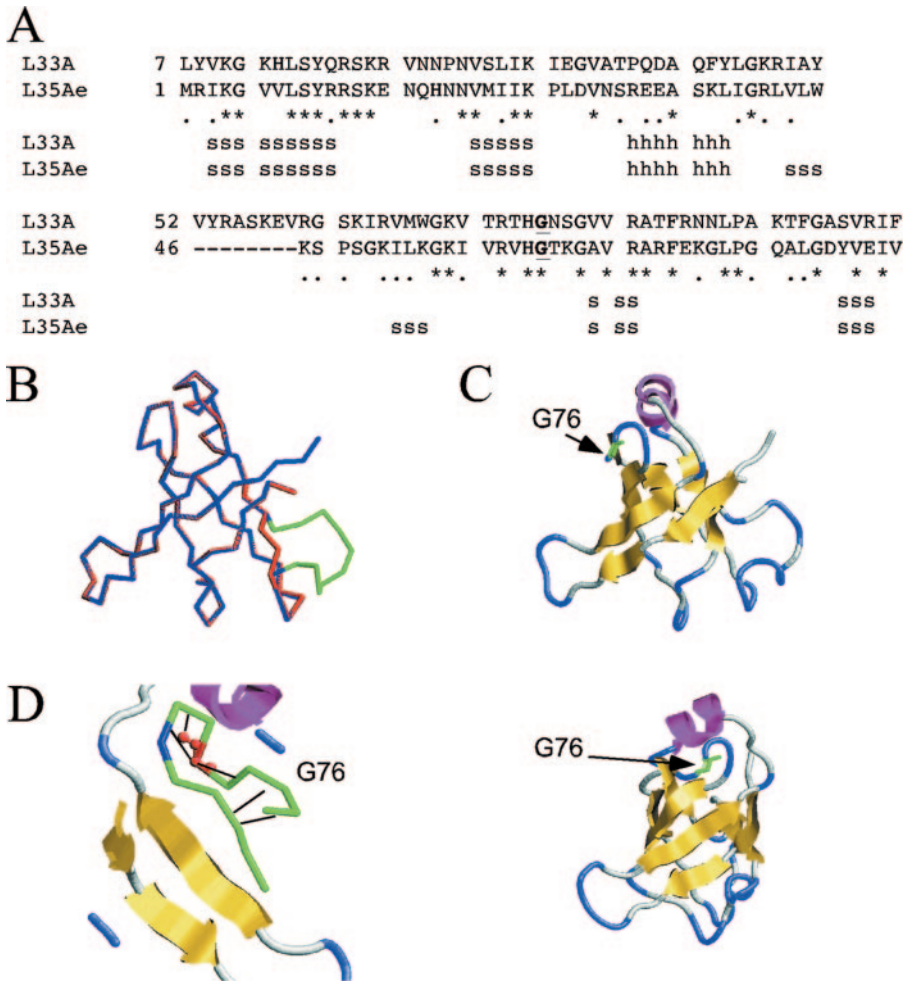

FIG. 2. Theoretical 3D model for rpL33. (A) Alignment of rpL33A's primary sequence with that of *Pyrococcus furiosus* 1SQR and secondary-structure predictions for rpL33. h, predicted alpha helix, s, predicted beta sheet. (B) Overlap of the main-chain backbones of 1SQR (blue) and rpL33A (red), showing a loop of rpL33A absent in 1SQR (green). (C) Predicted β-barrel 3D structure of rpL33 (yellow), with the position of an α-helix (dark pink) and of the G76R mutation in *rpl33a-G76R* (green). The diagram shown in panel B and the diagram in the upper portion of panel C are in the same orientation, and that in the bottom of panel C is rotated 90° to the right. (D) Glycine 76 (red) is predicted to form hydrogen bonds inside a rigid loop; its primary sequence is part of the 22-amino-acid carboxy-terminal domain conserved in the 99 members of the r-protein L35Ae family.

Structural features of rpL33 and prediction of a three-dimensional (3D) model. rpL33 is a small basic protein of 106 amino acid residues (excluding the N-terminally acetylated methionine that is processed) with orthologs in archaeabacteria (like L35Ae of *Pyrococcus furiosus*) and eukaryotes (like L32 of *Xenopus* spp. and L35a of rat and human) but not in bacteria. Interestingly, the *rpl33a-G76R* mutation maps to a motif of 22 amino acids that belongs to a putative RNA-binding domain located in the carboxy-terminal region of rpL33A and is well conserved in the 99 members of the "ribosomal protein L35Ae family" (http://www.ebi.ac.uk/interpro/IEntry?ac=IPR001780). However, the position of rpL33 in the cryo-electron microscopy structure of the yeast 80S ribosome has not been determined (63).

The nuclear magnetic resonance structure of the orthologous 50S r-protein L35Ae from the archaebacterium *Pyrococcus furiosus* (36% identity) has been obtained (62). We generated a theoretical model of the 3D structure of rpL33A using the coordinates of 1SQRm1.pdb for L35Ae and the ProModII program (N. Guex and M. C. Peitsch, SWISS-MODEL server). The sequence alignment of rpL33A with L35Ae and secondary-structure predictions are shown in Fig. 2A. Superposition of the main-chain backbones of the two proteins revealed only an extra loop in rpL33A, as shown in Fig. 2B. The predicted 3D structure of rpL33A, shown by a ribbon depiction in Fig. 2C, exhibits a β-barrel, one α-helix, and several long loops and turns. The G76R mutation alters a rigid loop close to the α-helix (Fig. 2D) and is not expected to disturb the overall structure of the protein (J. de las Rivas, personal communication).

The *rpl33a-G76R* mutation causes severe defects in polysome assembly. Because rpL33 is an essential constituent of the 60S ribosomal subunit, we investigated whether the *rpl33a-G76R* mutation causes defects in the general translation of mRNAs. To that end, we analyzed total polysome profiles from WT and mutant *rpl33a-G76R* strains by fractionating WCE on

sucrose gradients by velocity sedimentation (see Materials and Methods). Consistent with a reduction in the rate of colony formation on solid medium at all temperatures, the *rpl33a-G76R* mutant grew in liquid YPD medium at 37°C with an approximately twofold decrease in the growth rate relative to that of WT H117 (*RPL33A*). Therefore, we analyzed polysome profiles after shifting mutant and WT cells from 28°C to 37°C for 2 and 4 h. Quantification of the profiles revealed nearly identical polysome-to-monosome (P/M) ratios in mutant (P/M ratio, 3.5) and WT (P/M ratio, 3.4) cells grown at 28°C to mid-logarithmic phase. However, the pool of free 40S ribosomal subunits was elevated and that of 60S subunits was moderately decreased in the mutant at 28°C, concomitant with the appearance of half-mers in the 80S monosome and disome (2-mer) peaks of the profiles (Fig. 3A, time zero graph). The presence of half-mers, which contain one or more 80S ribosomes plus a 43S preinitiation complex (PIC) in the mRNA leader (34), is a hallmark of a reduced level of 60S subunits (56) resulting in a delay in 60S-subunit joining at the last step of translation initiation (23). When cells were grown to mid-logarithmic phase at 28°C and then incubated for 2 or 4 h at 37°C, the WT strain showed very little difference in polysome content (Fig. 3A, top panels). In contrast, after incubation at 37°C, the *rpl33a-G76R* mutant showed a notable reduction in the P/M ratio and a decrease in the average size of the polysomes compared to what was seen in WT cells. Half-mers are still observed in the monosome peaks of the mutant profiles, and the reduction in the 60S subunit is more apparent after 2 and 4 h of incubation at 37°C (Fig. 3A, bottom panels).

Quantification of total ribosomal subunits in low-Mg^{2+} sucrose gradients, where polysomes and 80S ribosomes dissociate to free subunits, revealed a deficit in 60S relative to 40S ribosomal subunits in the *rpl33a-G76R* mutant (Fig. 3B). A nearly constant ratio of 60S subunits to 40S subunits of ~1.70 was observed in the WT strain at 28°C and 37°C; however, the 60S/40S rRNA ratio was only 1.36 for the *rpl33a-G76R* mutant at 28°C and diminished further to 1.22 after 4 h at 37°C. Independent measurements of the 25S/18S rRNA ratios with an Agilent bioanalyzer revealed that the levels of rRNAs were nearly constant in the WT strain H117 (~1.6) but decreased in the *rpl33a-G76R* strain with incubation at 37°C (from ~1.0 at 28°C to 0.7 after 4 h at 37°C) in a manner similar to a reduction in the ratio of 60S subunits to 40S subunits (Fig. 3B). A moderate decrease in the total amount of 40S ribosomal subunits per A_{260} unit of extract was also observed in the *rpl33a-G76R* mutant under these conditions (Fig. 3B, bottom panels), as reported for other yeast mutants impaired in 60S-subunit production (73).

Together, the data in Fig. 3 suggest that the slow-growth phenotype of the *rpl33a-G76R* mutant results at least partially from a reduction in the level of 60S subunits, with a concomitant decrease in the rate of 60S-subunit joining that reduces the rate of general protein synthesis. Consistent with this, the rate of incorporation of radioactive methionine into acid-insoluble material was decreased by ~45% at 28°C and by 60% after 6 h of incubation at 37°C in *rpl33a-G76R* cells compared to that of isogenic *RPL33* cells (Table 2).

Defects in pre-rRNA processing caused by the *rpl33a-G76R* mutation. Mutations in genes for *trans*-acting factors involved early in the assembly of 60S subunits may cause some disassembly of early pre-60S ribosomal particles and attendant destabilization of pre-rRNA intermediates (reviewed in reference 41). Because some of those factors are believed to promote the correct folding of pre-rRNAs or the correct assembly of r-proteins, the mutations lead to defects in pre-rRNA processing and stability as secondary consequences (73). In the same manner, it is conceivable that the assembly of the mutant rpL33a-G76R protein into 60S preribosomes impairs the processing or stability of the pre-rRNAs that give rise to 25S rRNA.

To investigate defects in the pre-rRNA maturation pathway caused by the *rpl33a-G76R* mutation, we conducted Northern analysis of pre-rRNA species in mutant and WT cells grown to mid-logarithmic phase at 28°C and transferred to 37°C for 2, 4, or 6 h (Fig. 4). The processing pathway of pre-rRNA in *S. cerevisiae* and the probes for Northern analysis are shown in Fig. 4A. Staining of the blot with methylene blue revealed that the proportion of stable RNA comprised of rRNA declined in the mutant throughout the time course at 37°C, with substantial reductions in the steady-state levels of 25S rRNA and smaller reductions in those of 18S rRNA (Fig. 4B). This suggests a stronger effect of the *rpl33a-G76R* mutation on the production and accumulation of rRNAs in the 60S pathway than in the 40S pathway, in accordance with the results shown in Fig. 3B.

The pre-rRNAs and rRNAs were quantified relative to the level of polymerase II (Pol II)-transcribed U3 RNA (Fig. 4D). Hybridization with probes 1 and 4 revealed that cleavage at A0-A1-A2 of the 35S pre-rRNA is defective in the *rpl33a-G76R* mutant. The steady-state levels of 35S were higher in the mutant than in the WT at 28°C and after 2 h at 37°C but not after 4 h and 6 h at 37°C. In addition, strong reductions were observed in the levels of 27SA2 pre-rRNA (~40%; probe 4) and 20S pre-rRNA (~60%; probe 3) after 4 h at 37°C. Accordingly, the 35S/27SA2 and 35S/20S rRNA ratios were elevated in the mutant. The reduction in levels of 27SA2 and 20S pre-rRNA species at 37°C is consistent with a reduced rate of cleavage at sites A0, A1, and A2 (Fig. 4A).

Hybridization with probe 6 (between processing sites E and C2) (Fig. 4A) revealed that the levels of 27S pre-rRNA species were also diminished by a factor of ~50% and that those of the 7S pre-rRNA species was reduced by ~70% in the *rpl33a-G76R* mutant relative to levels in the WT after 4 h at 37°C (Fig. 4C). However, the 27SA2/25S and 27S/25S rRNA ratios were higher in the mutant than in the WT, suggesting that their processing is slower in the mutant, leading to lower rates of 25S and 5.8S rRNA production.

Another three pre-rRNA species were detected in samples of the *rpl33a-G76R* mutant, whose potential structures are depicted in Fig. 4E. First, 23S pre-rRNA was visualized with probes 1 and 4 in samples of the H275 mutant and of isogenic WT H117 (Fig. 4C). In yeast, alternative processing at A3 versus A2 seems to depend at least partly on the strain background (reference 24 and references therein). The 23S pre-rRNA accumulated ~1.5-fold at 28°C but diminished progressively during the incubation at 37°C in *rpl33a-G76R* cells. Second, an anomalous rRNA species that migrates just above 23S and below 25S in WT samples was visualized with probes 1, 4, and 6, while in mutant samples it suffers a progressive change of mobility during the incubation at 37°C, which al-

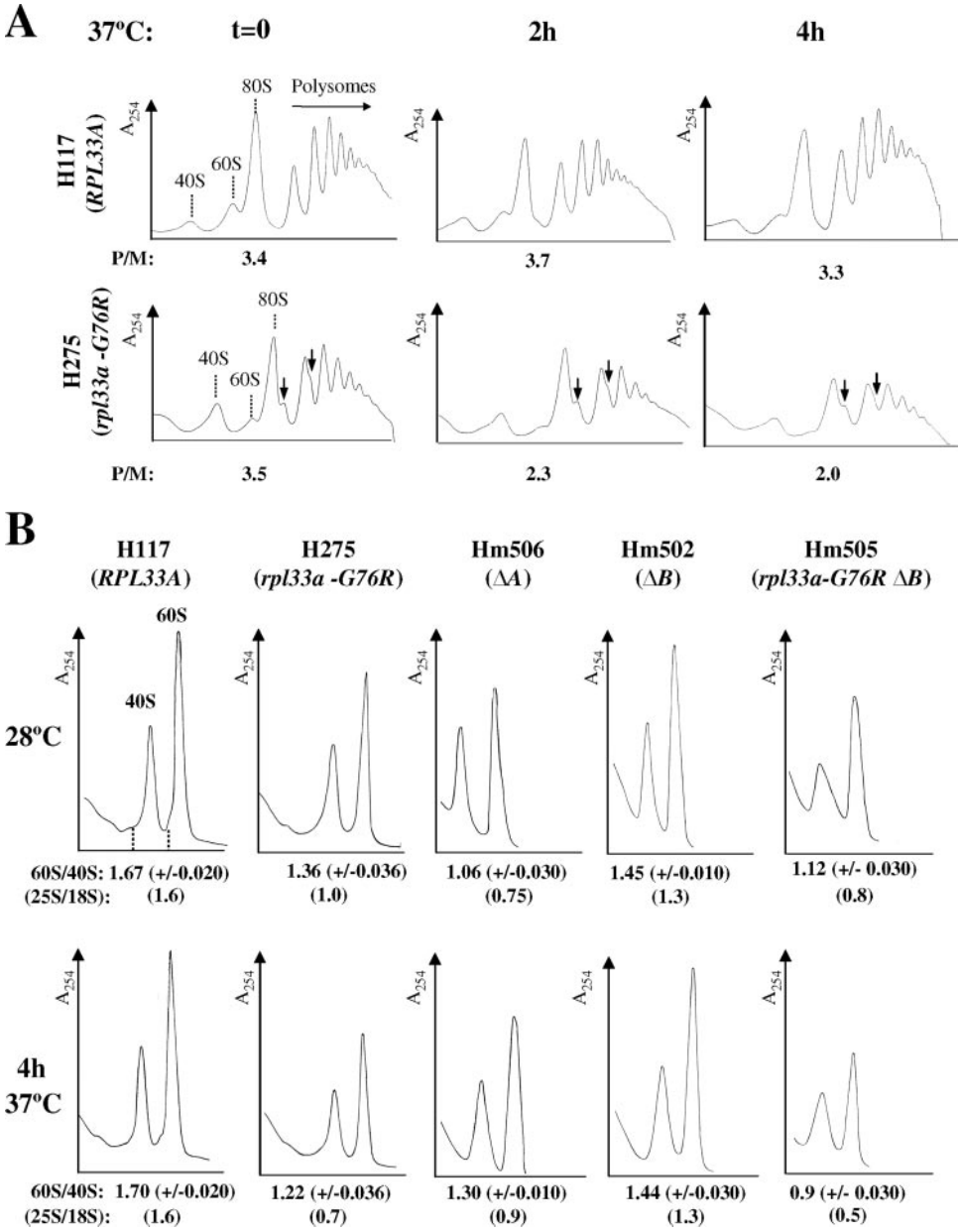

FIG. 3. The *rpl33a-G76R* mutation leads to a shortage in 60S ribosomal subunits and to the accumulation of half-mer polysomes. (A) The *rpl33a-G76R* strain H275 (bottom panels) and the isogenic *RPL33A* WT strain H117 (top panels) were grown in YPD to mid-logarithmic phase at 28°C (OD_{600}, ~0.8) and then shifted for 2 or 4 h at 37°C. Cycloheximide was added at 100 μg/ml before harvesting of cells, and WCE containing ribosomes and polyribosomes were prepared in the presence of 30 mM Mg^{2+} and separated by velocity sedimentation on 7% to 50% sucrose gradients. In the top panels, peaks representing free-ribosomal 40S and 60S subunits and 80S monosomes are indicated, and half-mer polysomes appearing in the H275 mutant profiles are marked by vertical arrows. The P/M ratios were calculated for profiles obtained from cells grown at 28°C (at time zero [graphs marked t = 0]) and after incubation at 37°C (graphs marked 2h and 4h), and the averages of values obtained in three independent experiments are indicated on the A_{254} tracings. (B) Strains H117 (RPL33A), H275 (*rpl33a-G76R*), Hm506 (Δ*A*), Hm502 (Δ*B*), and Hm505 (*rpl33a-G76R* Δ*B*) were cultured as described for panel A, but WCE were prepared in the absence of cycloheximide and Mg^{2+} and resolved by velocity sedimentation through 7% to 50% sucrose gradients. The mean ratios of total 60S/40S subunits determined from three replicate experiments are indicated below the A_{254} tracings, and the 25S/18S rRNA ratios estimated with an Agilent Technologies model 2100 bioanalyzer are indicated inside parentheses below the 60S/40S rRNA ratios.

lowed its identification (Fig. 4C). A similar "<25S" species was detected in other WT yeast strains, but its identity was not investigated further (i.e., see references 22 and 40). Based on our hybridization data, we deduced that the <25S species would be produced in our *gcn2-101 gcn3-101* genetic background by alternative processing at C2 when 35S pre-rRNA was not yet cleaved at A0-A1-A2 (Fig. 4A). A third anomalous species was detected with probe 1 in *rpl33a-G76R* at 37°C that may correspond to a 22.5S precursor produced by the cleavage of 35S or 23S pre-rRNAs at site D (9). This precursor is seen

TABLE 2. Rates of protein synthesis in *rpl33* mutants

Strain	Relevant genotype (37°C)	L-[^{35}S]methionine incorporation (cpm/10^3 cells/OD_{600}) at[a]:		
		0 h	3 h	6 h
H117	*gcn2 gcn3*	75.5 (±0.5)	31 (±2.0)	51 (±2.0)
H275	*gcn2 gcn3 rpl33a-G76R*	40 (±1.4)	17 (±1.4)	20 (±0.7)
Hm506	*gcn2 gcn3 ΔA*	51 (±2.0)	25 (±1.0)	31 (±2.4)
Hm502	*gcn2 gcn3 ΔB*	71 (±2.0)	29 (±2.0)	41 (±0.9)
Hm505	*gcn2 gcn3 rpl33a-G76R ΔB*	32 (±2.0)	10 (±2.0)	12 (±2.0)

[a] Values are averages of results obtained from two or three independent experiments (standard errors are shown inside parentheses).

only in the mutant at 37°C, suggesting that in *rpl33a-G76R* cells, processing at site D occurs when early processing at A0-A1 is inhibited (22, 52).

Analysis of low-molecular-weight rRNA species of the 60S subunit in the same blot revealed that levels of 5.8S rRNA (probe 5) were diminished by ~30% in the *rpl33a-G76R* mutant relative to levels in the WT after 4 h at 37°C. However, the ratio of 7S rRNA to 5.8S rRNA was slightly lower in the mutant than in the WT, indicating that this processing reaction is not affected by *rpl33a-G76R*. Notably, levels of Pol III-transcribed 5S rRNA (probe 8) were reduced in the same proportion as 5.8S rRNA in mutant cells (Fig. 4C). The 5S rRNA is short-lived, probably reflecting its lack of nucleotide modification, unless it is complexed with yeast rpL5 (12). Thus, perhaps a fraction of 5S rRNA is degraded because its rate of assembly into the corresponding preribosomal 60S particles is reduced in *rpl33a-G76R* cells.

Finally, in the 40S maturation branch, there was a greater reduction in the level of 20S pre-rRNA (~60%; probe 3) than of 18S rRNA (~40%; probe 2) in the mutant after 4 h at 37°C (Fig. 4C), suggesting that processing of 20S to 18S rRNA is normal in *rpl33a-G76R* cells.

In summary, the Northern analysis revealed multiple defects indicative of impaired processing of 35S pre-rRNA at sites A0-A1-A2 that would contribute to the reduced production of both 25S and 18S rRNAs in *rpl33a-G76R* cells at the restrictive temperature. It appears that the reduction is more severe for 25S rRNA because of additional defects in 27S to 25S rRNA processing and to the instability of the 27SA2 precursor. Together, these data support the notion that rpL33 is required early in the ribosome biogenesis pathway for correct and efficient processing and for the optimal stability of several pre-rRNA species and, hence, the normal accumulation of the four mature rRNAs. It is possible, however, that defective biogenesis of the 60S rRNA has an indirect effect on the early processing of 35S pre-rRNA at A0-A1-A2 (73). Substantial reductions in the steady-state levels of mature 25S, 5.8S, and 5S rRNAs are consistent with the severe deficit of 60S subunits observed in the polysome profiles of the *rpl33a-G76R* mutant. The strong decrease in levels of 60S subunits and the less severe reduction in 40S subunits most likely contribute to the translation defect and Slg$^-$ phenotype of the *rpl33a-G76R* mutant.

Phenotype of reduced dosage of WT rpL33 compared to that of the *rpl33a-G76R* mutant. The Slg$^-$ phenotype of *rpl33a-G76R* mutants is recessive in heterozygous diploids (*rpl33a-G76R*/*RPL33A*), probably due to the loss of rpL33A function in rRNA maturation and 60S biogenesis. In contrast, the Gcd$^-$ phenotype of *rpl33a-G76R* shows dominance, as noted above, suggesting an alteration in rpL33A function in translation initiation. We investigated whether a reduced dosage of WT rpL33, due to chromosomal deletion of *RPL33A* or *RPL33B*, leads to a Gcd$^-$ phenotype in the *gcn2-101 gcn3-101* background and whether the deletions impact 60S subunit biogenesis to the extent observed for the *rpl33a-G76R* mutation. First, total RNAs obtained from the single-deletion mutants Hm506 (*rpl33a*::*URA3 RPL33B* [Δ*A*]) and Hm502 (*RPL33A rpl33b*::*kanMX4* [Δ*B*]) were subjected to Northern analysis, using a genomic probe that hybridizes to both *RPL33A* and *RPL33B* mRNAs (Materials and Methods). Quantification of the hybridization signals relative to those of the Pol III-transcribed *SCR1* RNA analyzed as an internal control revealed that the steady-state levels of *RPL33A* mRNA in the Δ*B* mutant is ~85% higher than that of *RPL33B* mRNA in the Δ*A* mutant (Fig. 5A). This result is in agreement with a previous quantification of β-galactosidase activity synthesized from *RPL33A-lacZ* and *RPL33B-lacZ* hybrid transcripts in deletion mutants constructed in another yeast genetic background (65) in which *RPL33A* expression was estimated to be sevenfold higher (86%) than that of *RPL33B* (~14%). Thus, Δ*A* and Δ*B* should have different consequences for cellular processes in which rpL33 is required, a prediction borne out by the growth phenotypes of the corresponding deletion mutants (Fig. 5B). Replacing *RPL33B* with the null allele *rpl33b*::*kanMX4* in strain H275 (*rpl33a-G76R*) generated the viable *rpl33a-G76R rpl33b*::*kanMX4* double mutant Hm505 (*rpl33a-G76R* Δ*B*), which has an Slg$^-$ phenotype similar to that of the *rpl33a-G76R* single mutant (Fig. 5B). Because rpL33 is essential, this result implies that the mutant protein rpL33a-G76R is assembled into mutant 60S subunits that are partially functional in translation.

We next compared the phenotypes of the *rpl33a-G76R* mutant, Δ*A* mutant, Δ*B* mutant, and a strain with the combined *rpl33a-G76R* and Δ*B* mutations on cell growth, ribosome biogenesis, and general protein synthesis. The *rpl33a-G76R* and Δ*A* mutations produce similar growth defects at 28°C, but *rpl33a-G76R* confers a more severe Slg$^-$ phenotype than does the Δ*A* mutation at 37°C (Fig. 5B). By contrast, the Δ*B* mutant grows indistinguishably from the WT at all temperatures. Notably, at 28°C, the *rpl33a-G76R* mutant exhibits a smaller reduction in the 60S/40S ratio (declining to 1.36 from the WT value of 1.67) than does the Δ*A* strain (ratio of 1.06) (Fig. 3B, time zero graph), thus indicating that the complete absence of rpL33A leads to a stronger 60S subunit biogenesis defect than does *rpl33a-G76R* at this temperature. However, after 4 h at 37°C, the 60S/40S ratio was lower in the *rpl33a-G76R* mutant

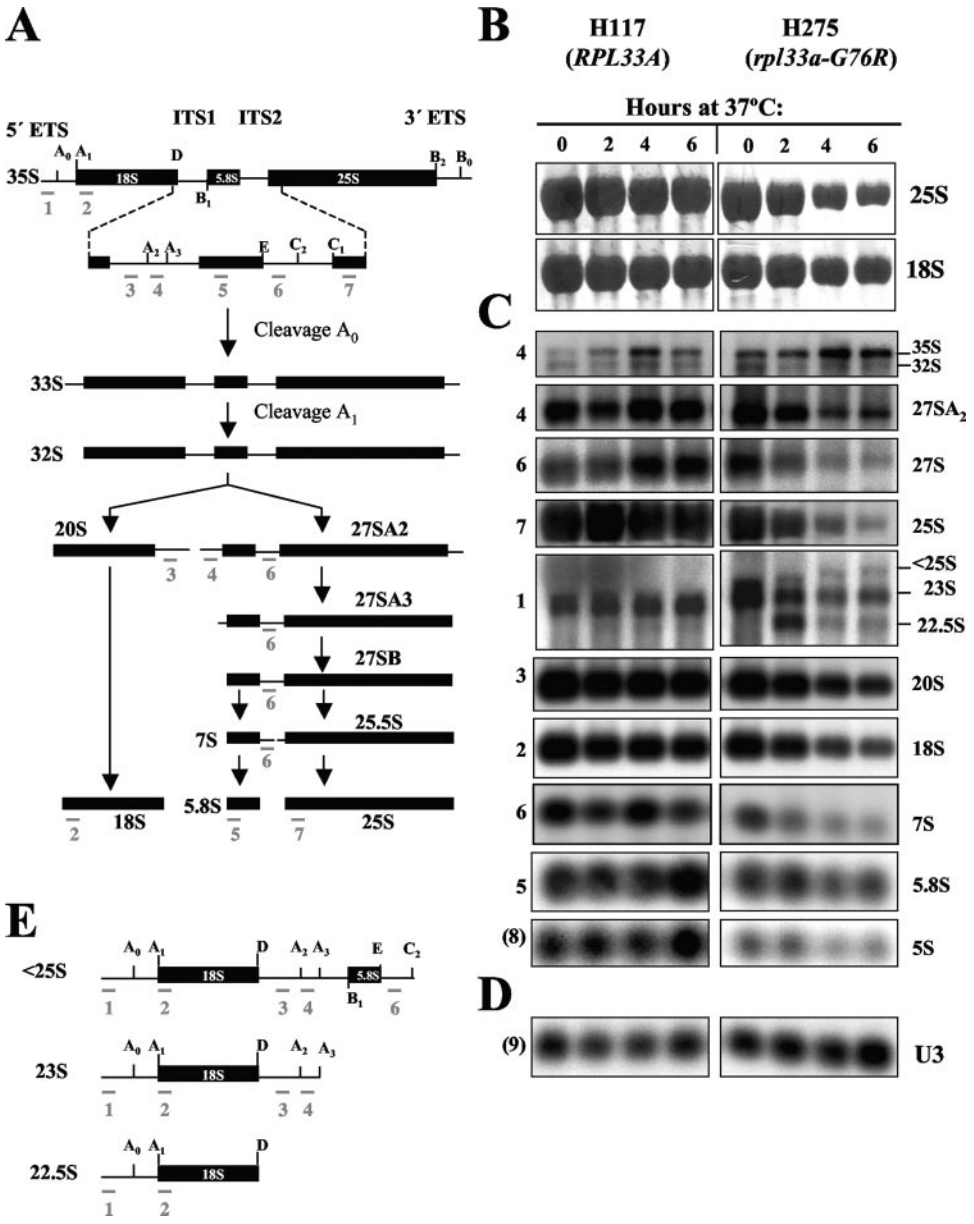

FIG. 4. Deficient and aberrant processing of pre-rRNAs in *rpl33a-G76R* cells shown by Northern analysis. (A) Scheme of the pre-rRNA processing pathway. The 35S pre-rRNA contains the sequences for mature rRNAs (18S, 5.8S, and 25S) separated by two internal transcribed spaces (ITS1 and ITS2) and flanked by two external transcribed spaces (5′ETS and 3′ETS). The rRNAs are shown as filled bars and the transcribed spaces represented as lines. The processing sites are indicated above the diagram by the uppercase letters A to E. The annealing positions of oligonucleotides 1 to 7 used as hybridization probes are indicated beneath all of the rRNA species that they detect. (B to D) Strains H117 (*RPL33A*) and mutant H275 (*rpl33a-G76R*) were cultured in liquid YPD medium at 28°C to mid-logarithmic phase (OD_{600}, ~0.8) and shifted to 37°C for 2, 4, or 6 h. Total RNA was extracted, and samples containing 10 μg were resolved on a 1.2% agarose–4% formaldehyde gel and subjected to Northern analysis. (B) The blot was first dyed with methylene blue to test the integrity of the 25S and the 18S rRNAs. (C) The blot was consecutively hybridized with probes whose positions are depicted in panel A. The RNA species, visualized with the probes indicated at the left, are labeled on the right. The probe specific for 5S rRNA is indicated as (8) (Materials and Methods). (D) Hybridization with a probe specific for U3 (9) (Materials and Methods), which was used as internal control for loading. (E) Schematic diagram showing the potential origin of aberrant and less common pre-rRNA species indicated in panel C.

(1.22) than in the Δ*A* mutant (1.3), showing that *rpl33a-G76R* impairs 60S subunit biogenesis to an extent comparable to that given by Δ*A* at the restrictive temperature of 37°C. As expected, the Δ*B* mutant exhibits 60S/40S ratios lower than that of the WT but higher than that of the Δ*A* mutant (Fig. 3B), indicating that the absence of rpL33B causes a less severe 60S subunit biogenesis defect than does Δ*A*. The *rpl33a-G76R* Δ*B* double mutant has a 60S biogenesis defect comparable to that of the Δ*A* mutant at 28°C but much more severe than that of the Δ*A* mutant at 37°C (Fig. 3B).

In contrast to the effects on ribosome biogenesis, *rpl33a-G76R* leads to a greater reduction in [^{35}S]methionine incorpo-

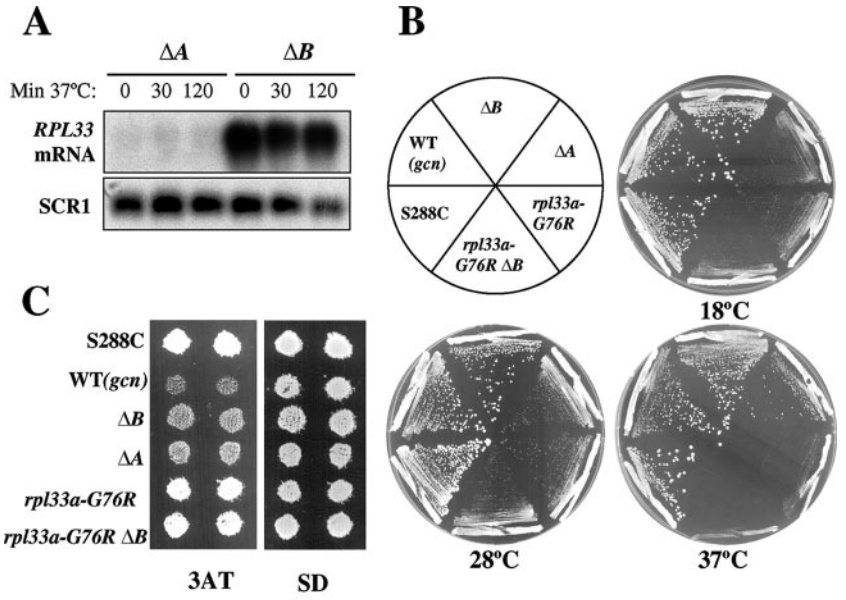

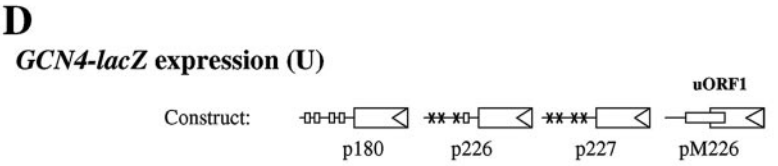

Strain	Genotype	R	DR	R	DR	R	DR	R	DR
H466	*gcn2 gcn3*	50	60	40	40	6900	5400	30	30
Hm526	*gcn2 gcn3 ΔA*	70	100	60	60	6400	6600	100	100
Hm527	*gcn2 gcn3 rpl33a-G76R*	170	170	120	140	4800	5800	200	190

FIG. 5. Comparison of the Gcd$^-$ and Slg$^-$ phenotypes of several rpl33 mutants. (A) Steady-state amounts of *RPL33* mRNAs. Cells of Hm506 (Δ*A*) and Hm502 (Δ*B*) were grown in YPD to mid-logarithmic phase at 28°C (OD_{600}, ~0.8) and transferred for 30 min or 2 h at 37°C. Total RNA was extracted and 10 μg analyzed by Northern blotting using a probe that hybridizes to both *RPL33A* and *RPL33B* mRNAs and a probe for SCR1, used as the loading control (10) (Materials and Methods). (B) The Slg$^-$ phenotypes of Hm502 (Δ*B*), Hm506 (Δ*A*), and Hm505 (*rpl33a-G76R* Δ*B*) mutants are shown relative to that of the original mutant H275 (*rpl33a-G76R*) and to the WT phenotype (Slg$^+$) of the parental strain H117 (*gcn2 gcn3 RPL33A RPL33B*). The Slg$^+$ phenotype of the WT strain S288C (*GCN2 GCN3 RPL33A RPL33B*) is shown as a reference. The growth phenotypes were analyzed by streaking single colonies on YPD medium and incubating the plates for 8 days at 18°C and for 3 days at 28°C or at 37°C. (C) The Gcd$^-$ phenotype (3AT^R) of the same mutants as those shown in panel B is shown relative to that of the original mutant H275 and to the 3AT^S (Gcn$^-$) phenotype of the parental strain H117. The 3AT^R phenotype of the WT strain S288C is shown as a reference. Isolated colonies of each strain were replica printed to 10 mM 3AT and to SD plates and incubated for 3 days at 28°C. (D) The *rpl33a-G76R* and Δ*A* mutations lead to constitutive derepression of *GCN4-lacZ* independently of the positive GCN regulators. *GCN4-lacZ* fusions were introduced into yeast strains on low-copy-number plasmids p180, p226, p227, and pM226 (labeled boxes with a triangle at the right end). The relevant genotypes of the strains are indicated on the left below these diagrams. The *gcn2-101 gcn3-101* strains H466 (*RPL33A*), Hm526 (Δ*A*), and Hm527 (*rpl33a-G76R*) are isogenic. The four uORFs in the leader sequence of p180 are shown as open boxes, and point mutations that remove the AUG codons of uORF1 to -3 (p226) or uORF1 to -4 (p227) are shown as ×s. uORF1 in pM226, located at the position of uORF4 and elongated to overlap the beginning of *GCN4*, is indicated by a rectangle. β-Galactosidase activity was measured in cells grown to mid-logarithmic phase under nonstarvation, repressing (R), or derepressing (DR) conditions of histidine starvation induced by 3AT. Values are averages of results obtained in three independent experiments with two independent transformants. Units of β-galactosidase activity were calculated as indicated in Materials and Methods.

ration than does Δ*A* at 28°C (Table 2). This difference was also observed at 37°C, but in this case it was consistent with the relative effects of the Δ*A* mutation and *rpl33a-G76R* on 60S subunit biogenesis (Fig. 3B). The *rpl33a-G76R* Δ*B* double mutant displays a much stronger reduction in protein synthesis than does the Δ*A* single mutant at 28°C, even though these two strains have comparable 60S subunit biogenesis defects at this temperature. At 37°C, the *rpl33a-G76R* Δ*B* double mutant exhibits the strongest defect of all in protein synthesis, commensurate with the most severe 60S subunit biogenesis defect observed for any of the mutants at this temperature (Table 2 and Fig. 3B, respectively). The facts that at 28°C the *rpl33a-G76R* and *rpl33a-G76R* Δ*B* mutants display defects in 60S subunit biogenesis that are less significant than or similar to

TABLE 3. Derepression associated with *rpl33* mutations of histidine-biosynthetic enzymes

Strain[c]	Relevant genotype	Growth on 3AT[a]	*HIS4-lacZ* activity (U)[b]	
			R conditions	DR conditions
H117	*gcn2 gcn3*	−	150	170
H275	*gcn2 gcn3 rpl33a-G76R*	++	670	530
Hm525	*gcn2 gcn3 ΔA*	+/−	270	400
Hm502	*gcn2 gcn3 ΔB*	−/+	210	240
Hm505	*gcn2 gcn3 rpl33a-G76R ΔB*	++	620	540
F3	*GCN2 GCN3*	++	100	800
Hm532	*GCN2 GCN3 rpl33a-G76R*	++	880	860
Hm531	*GCN2 GCN3 ΔA*	+	240	300

[a] Strains were replica printed to 3AT (10 mM) medium and scored for growth at 28°C after 3 days. ++, confluent growth; +/− and −/+, weak and very weak growth, respectively; −, no visible growth.

[b] β-Galactosidase activity was assayed under repressing (R; nonstarvation) and derepressing (DR; histidine starvation) conditions. Values are averages of results obtained from three independent experiments with two or three independent transformants.

[c] All strains were isogenic.

those of the Δ*A* mutant, but reductions in methionine incorporation were significantly larger than in the Δ*A* mutant at this temperature suggest that altering rpL33A with G76R impairs translation more strongly than does the elimination of rpL33A by Δ*A*.

Strong evidence supporting the last conclusion came from comparing the Gcd$^-$ phenotypes of the *rpl33a-G76R* and Δ*A* mutants. As shown in Fig. 5C, the Δ*A* mutation leads to a weak Gcd$^-$ phenotype in Hm506 (3AT^R/3AT^S), showing lower 3AT resistance than that conferred by *rpl33a-G76R* in the isogenic H275 mutant, even though the two mutants exhibit nearly identical Slg$^-$ phenotypes at 28°C on rich medium (Fig. 5B) and minimal medium (data not shown). This result implies that at 28°C, *rpl33a-G76R* produces an additional defect in translation initiation that elicits greater derepression of *GCN4* translation than does the Δ*A* mutation. The Δ*B* mutation also confers a weak Gcd$^-$ phenotype (3AT^S/3AT^R), suggesting that it reduces rpL33 levels enough to weakly derepress *GCN4* but not enough to significantly affect general protein synthesis.

To quantify the strength of the Gcd$^-$ phenotype conferred by each mutation in *gcn2-101 gcn3-101* cells at 28°C, we first measured the β-galactosidase activity expressed from a *HIS4-lacZ* fusion integrated at the *URA3* locus of the mutant and WT strains (Table 3). In the absence of amino acid starvation, the β-galactosidase activity was ~4.5-fold higher in *rpl33a-G76R* mutant than in WT cells but only ~2-fold higher in Δ*A* cells, indicating that the rpL33a-G76R mutant protein has a stronger effect on *HIS4-lacZ* expression than does the complete absence of rpL33A. As expected, the absence of rpL33B (Δ*B*) increased *HIS4* expression by the least amount, only ~1.5-fold relative to the level expressed in H117, but did not exacerbate the derepression produced by *rpl33a-G76R* in the double mutant. Under amino acid starvation conditions (Table 3), the values of β-galactosidase were similar to those measured in the absence of starvation, indicating that the *rpl33a-G76R*, Δ*A*, and Δ*B* mutations constitutively derepress *HIS4-lacZ* expression in *gcn2 gcn3* cells (Gcd$^-$ phenotype).

We also measured the β-galactosidase activity synthesized from a *HIS4-lacZ* fusion integrated at the *URA3* locus of the *GCN2 GCN3* WT strain F35 (*RPL33A*) and of isogenic Hm531 (Δ*A*) and Hm532 (*rpl33a-G76R*) mutants generated in the same *GCN* background (Table 3). As expected, the values of β-galactosidase were approximately eightfold higher under starvation conditions than under nonstarvation conditions in WT strain F35. Nearly identical high levels of β-galactosidase activity were observed in the *rpl33a-G76R* mutant under both repressing and derepressing conditions, indicating that this mutation constitutively increases *HIS4-lacZ* expression in *GCN* cells to an extent similar to that given by starvation in isogenic WT cells. In contrast, Δ*A* increased *HIS4-lacZ* expression by a much smaller amount under repressing and derepressing conditions. These data confirm that *rpl33a-G76R* elicits much stronger derepression of a GCN4 target gene than does Δ*A* at 28°C.

To obtain direct evidence that *rpl33a-G76R* and the Δ*A* mutations derepress *GCN4* expression at the translational level, we measured β-galactosidase expression from a plasmid-borne *GCN4-lacZ* fusion in the isogenic *gcn2-101 gcn3-101* strains H466 (*RPL33A*), Hm526 (Δ*A*), and Hm527 (*rpl33a-G76R*) grown at 28°C. The fusion construct in p180 contains the WT *GCN4* mRNA leader with the four uORFs and, thus, exhibits WT translational regulation of *GCN4* expression (49). As shown in Fig. 5D, low-level expression of *GCN4-lacZ* on p180 was observed in the WT strain H466 under nonstarvation and histidine starvation conditions, because the *gcn2-101 gcn3-101* alleles present in this strain impair derepression of *GCN4* translation (36). The *rpl33a-G76R* mutation led to *GCN4-lacZ* expression in Hm527 at levels ~3-fold greater than those observed in H466, whereas Δ*A* in Hm526 produced only ~1.5-fold greater expression. These results, together with those in Tables 2 and 3 described above, indicate that the *rpl33a-G76R* mutation impairs 60S subunit function in translation initiation in a manner distinguishable from a simple reduction in the abundance of 60S subunits. Given that 60S subunits participate only at the last step of 80S initiation complex assembly, it is likely that *rpl33a-G76R* impairs 60S-subunit joining to the 48S PIC.

The derepression of *GCN4* translation under amino acid starvation requires uORF1, so that *GCN4-lacZ* expression is low and unregulated from the construct in p226 containing uORF4 alone in WT cells (Fig. 5D) (49). Interestingly, *rpl33a-G76R* increased the expression of the p226 construct approximately threefold compared to that seen in WT strain H466 under repressing and derepressing conditions, whereas Δ*A* led to a smaller increase of less than twofold. These findings sug-

gest that the derepression of *GCN4-lacZ* expression conferred by *rpl33a-G76R* and Δ*A* results from leaky scanning of uORF4 by fully assembled PICs (i.e., containing the TC) because of a defect in subunit joining. (The term leaky scanning signifies the bypass of an AUG codon by a scanning PIC and does not refer to the nature of the scanning process at sequences preceding the start codon.) However, this effect could also arise from increased reinitiation following uORF4 termination. To distinguish between these two possibilities, we measured *GCN4-lacZ* expression from the pM226 construct in which uORF1 is the sole uORF, located in the position of uORF4 and elongated to overlap the beginning of *GCN4* (31). Mutations that cause leaky scanning would increase *GCN4-lacZ* expression from pM226, whereas a mutation that allowed increased reinitiation after terminating at uORF4 would not affect the expression of this construct. As shown in Fig. 5D, pM226 gives very low expression in WT cells, because the ribosomes cannot reinitiate after terminating at the elongated version of uORF1 far downstream from the *GCN4* AUG codon. In contrast, *rpl33a-G76R* increased the expression of the pM226 construct approximately sevenfold compared to that seen in WT strain H466, under repressing and derepressing conditions, and Δ*A* led to a smaller increase of less than fourfold, consistent with increased leaky scanning of uORF1 in the two mutants.

Finally, if rpL33A represses the translation of *GCN4* via the uORFs, eliminating all of them should abolish the derepressing effect of the *rpl33a-G76R* and Δ*A* mutations on *GCN4-lacZ* expression. Consistent with this prediction, *rpl33a-G76R* and Δ*A* had little effect on the expression of the *GCN4-lacZ* construct lacking all four uORFs (p227), thus indicating that rpL33 regulates *GCN4* expression at the translational level via the uORFs. Together, these data show that rpL33A is required for the repression of *GCN4* translation under conditions of amino acid sufficiency by preventing leaky scanning of the uORFs, most likely by ensuring efficient 60S-subunit joining.

Genetic partners of rpL33. To discover possible interactions of rpL33 with other components of the pre-60S particles, we tested for functional suppression of the *rpl33a-G76R* mutation by overexpressing *NOP7*, which encodes a nucleolar protein essential for the biogenesis of the 60S subunit (1). The *nop7-1* mutation or depletion of NOP7 leads to pre-rRNA processing defects similar to those described above for *rpl33a-G76R* mutants (1), and rpL33 copurifies with TAP-NOP7 (33). The *nop7-1* mutation was identified in a genetic screen for mutations synthetically lethal with *drs1* mutations (1). *DRS1* encodes a DEAD box RNA helicase required for 60S subunit biogenesis (54), and most of the *drs1* mutants are defective in the processing of 27S pre-rRNA to 25S rRNA (1, 6, 54). Overexpression of *NOP7* or *DRS1* (Materials and Methods) weakly suppressed the Slg$^-$ phenotype at 37°C but not the 3AT^R phenotype of the *rpl33a-G76R* mutant Hm337 (Fig. 6A). Conversely, the hc*RPL33A* plasmid suppressed the Slg$^-$ phenotype produced by *nop7-A* at 28°C and 18°C (Fig. 6B) and that produced by *nop7-C* and *nop7-F* but not that produced by 10 other *nop7* mutations (data not shown). The same test was conducted with the hc*RPL33A* plasmid on several *drs1* mutants (*drs1-1*, *-3*, *-5*, and *-6* mutants) (1). Only the Slg$^-$ phenotypes at 28°C of the *drs1-1* (Fig. 6B) and *drs1-6* (not shown) mutants were suppressed by overexpressing rpL33A. The allele-specific suppression of the *nop7* and *drs1* mutations by rpL33A overexpression observed here may indicate functional or physical interactions of rpL33A with two nucleolar proteins required for essential steps leading to the synthesis of 60S ribosomal subunits. rpL33A might facilitate the function of NOP7 in the exonucleolytic processing of the 27SA3 pre-rRNA to later processing intermediates and the mature 5.8Ss rRNA or stimulate the function of DRS1 in the production of 25S rRNA from 27S pre-rRNAs.

Furthermore, we identified the gene encoding the poly(A) binding protein (*PAB1*) as a dosage suppressor of the Slg$^-$ phenotype of the *rpl33a-G76R* and Δ*A* mutants (Fig. 6C and data not shown). However, the hc*PAB1* strain did not suppress the 3AT^R/Gcd$^-$ phenotypes of the *rpl33a-G76R* and Δ*A* mutants (Fig. 6D and data not shown). It also did not suppress the Slg$^-$ phenotypes conferred by mutations that reduce the assembly of the TC, including the *gcd11-505* mutation in the γ subunit of eIF2, the *gcd1-501* mutation in the γ subunit of eIF2B (the GEF for eIF2), and the *gcd14-2* mutation in the catalytic subunit of the methyltransferase that modifies position 58 in tRNA$_i^{Met}$ (data not shown). Accordingly, we considered the possibility that the hc*PAB1* plasmid only reduces the deficiency in ribosomal subunits in the *rpl33a-G76R* and Δ*A* mutants. In agreement with this idea, we found that PAB1 overexpression leads to increased levels of both 25S and 18S rRNAs at 28°C in *rpl33a-G76R* cells, leaving a moderate deficit in 25S rRNA versus 18S rRNA steady-state levels (see Fig. S1A and B in the supplemental material). Thus, the hc*PAB1* plasmid should increase the amounts of 60S and 40S subunits, without eliminating a relative deficiency in 60S subunits, in *rpl33a-G76R* cells. Importantly, hc*PAB1* did not reduce significantly the abundance of half-mers observed in the polysome profiles of the *rpl33a-G76R* mutant (see Fig. S1C in the supplemental material). The last finding, together with the failure of the hc*PAB1* plasmid to reduce the Gcd$^-$ phenotype, indicates that a strong subunit joining defect persists in *rpl33a-G76R* cells overexpressing PAB1 despite the elevated levels of ribosomal subunits. This reinforces our conclusion that *rpl33a-G76R* confers a specific defect in subunit joining apart from its effect in reducing 60S-subunit levels.

Finally, we found that overexpressing tRNA$_i^{Met}$ from a high-copy-number plasmid containing the *IMT4* gene (hc*IMT4*) suppressed the 3AT^R phenotypes of *rpl33a-G76R* and Δ*A* cells but not the corresponding Slg$^-$ phenotypes. Similar results were obtained for a high-copy-number plasmid encoding the three subunits of eIF2 in addition to *IMT4* to achieve overexpression of the TC (Fig. 6C and D). To explain these results, we propose that the delay in subunit joining at the uORF4 AUG codon in *rpl33a* mutants leads to the dissociation of tRNA$_i^{Met}$ from the 40S subunit and allows the resumption of scanning from uORF4 to *GCN4* as the basis for the Gcd$^-$ phenotypes of these mutants. In this view, raising the concentration of tRNA$_i^{Met}$ would increase the occupancy of the TC on the stalled 40S subunits and thereby prevent their leaky scanning of the uORF4 AUG codon. As this would not correct the defect in ribosome biogenesis and subunit joining defects in these mutants, this model can explain why the hc*IMT4* plasmid does not suppress the Slg$^-$ phenotypes of the *rpl33a-G76R* and Δ*A* mutants.

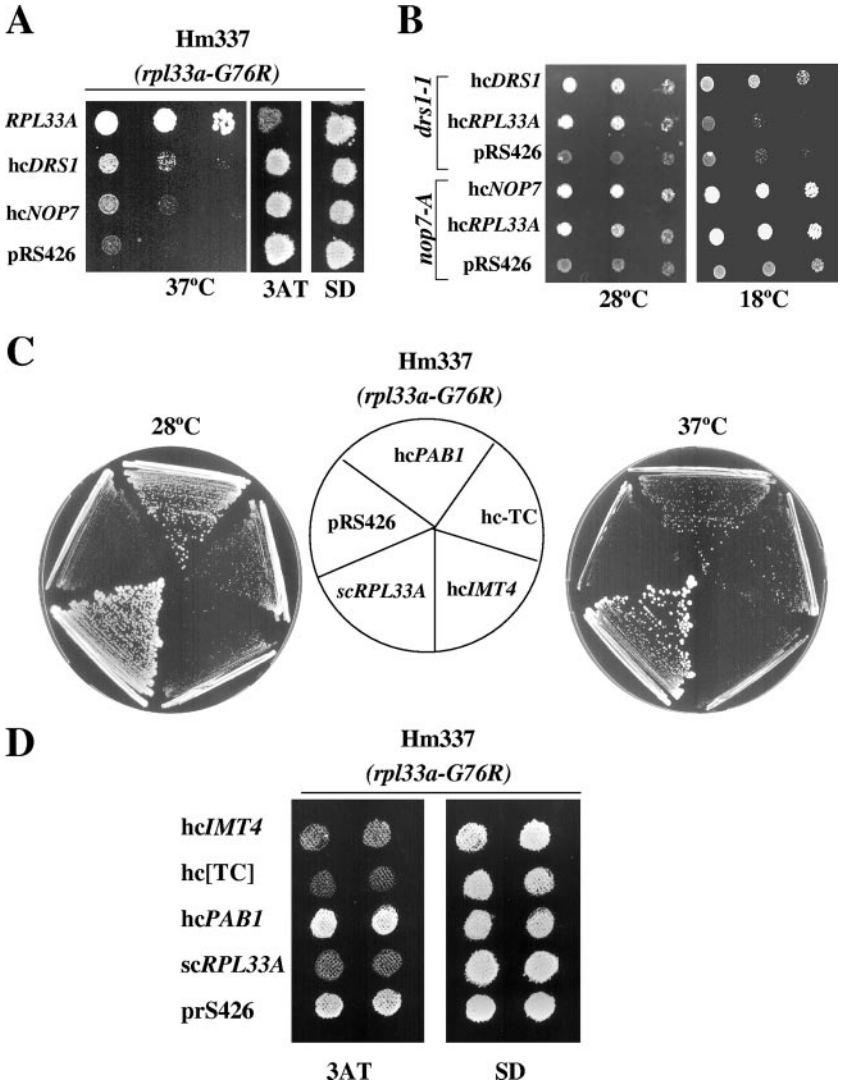

FIG. 6. Genetic interactions of *rpl33a-G76R*. (A) Weak suppression of *rpl33a-G76R* by hc*NOP7* and hc*DRS1* plasmids. Transformants of the Hm337 mutant (*rpl33a-G76R*) carrying an empty vector (pRS426) or high-copy-number plasmids bearing *RPL33A* (pPM13), *NOP7* (pJW6039), or *DRS1* (pJW3015) were grown in SD-Ura medium at 28°C and serial dilutions (10^3 to 10 cells) plotted on plates of the same medium, which were incubated for 3 days at 37°C (left panel). Isolated colonies of each transformant were replica printed to plates containing 10 mM 3AT and to minimally supplemented SD plates and incubated for 3 days at 28°C (right panels). (B) Allele-specific suppression of the *nop7* and *drs1* mutations by the hc*RPL33A* plasmid. Mutant *drs1-1* and *nop7-A* strains bearing an hc*RPL33A* plasmid (pPM13), empty vector (pR8426), or high-copy-number plasmids bearing *DRS1* (pJW3015) or *NOP7* (pJW6039) were grown as described for panel A and plotted on SC-Ura plates, which were incubated for 2 days at 28°C or for 5 days at 18°C. (C) Dosage suppressors of the Slg$^-$ phenotype of the *rpl33a-G76R* mutant. Transformants of Hm337 (*rpl33a-G76R*) carrying an empty vector (pRS426), a single-copy plasmid bearing *RPL33A* (pPM2), or high-copy-number plasmids bearing *RPL33A* (pPM13), *PAB1* (pAS425), *IMT4* (p2635), or the three subunits of eIF2 plus *IMT4* (hc-TC; p3000) were streaked for single colonies on minimally supplemented SD medium and incubated at 28°C (3 days) or 37°C (4 days). (D) The Gcd$^-$ phenotype of *rpl33a-G76R* is partially suppressed by the hc*IMT4* plasmid and the hc-TC, but not by the hc*PAB1* plasmid. Isolated colonies of the same transformants as those described in panel C were replica printed to plates containing 10 mM 3AT and to SD plates and incubated for 3 days at 28°C.

DISCUSSION

In this report, we have shown that the *rpl33a-G76R* mutation in *RPL33A* leads to a defect in 60S-ribosomal-subunit accumulation and constitutive derepression of *GCN4* translation. It was shown previously that reducing the concentration of 60S subunits by deleting *RPL16B* (currently named *RPL11B*) produced a moderate Gcd$^-$ phenotype, partially derepressing the expression of *GCN4* and its target gene *HIS4* (23). Thus, it was possible that *rpl33a-G76R* confers a Gcd$^-$ phenotype simply by decreasing rpL33A abundance or preventing its incorporation into 60S subunits, with attendant reduction in the 60S-subunit concentration. However, *rpl33a-G76R* confers a much stronger Gcd$^-$ phenotype than does the deletion of *RPL33A*, producing greater resistance to 3AT and more-extensive derepression of *GCN4-lacZ* and *HIS4-lacZ* expression. Importantly, the stronger Gcd$^-$ phenotype of *rpl33a-G76R* was evident at 28°C, at which temperature it produces a less severe reduction in 60S-subunit accumulation than does Δ*A*. Furthermore, *rpl33a-G76R* produces a greater

reduction in the rate of methionine incorporation than does Δ*A* at 28°C. Together, these findings suggest that *rpl33a-G76R* alters the function of rpL33A in a way that impairs translation initiation and *GCN4* translational control more dramatically than does a simple reduction in rpL33A abundance. Given that the 60S subunit does not participate in translation initiation until the subunit joining step, it is likely that *rpl33a-G76R* alters the 60S subunit in a way that impedes the joining reaction. We propose that subunits containing the *rpl33a-G76R* product are impaired for subunit joining and that they compete with the functional subunits containing rpL33B. (The partial dominance of its Gcd$^-$ phenotype shows that competition by defective subunits containing *rpl33a-G76R* is evident even in the presence of WT rpL33A in heterozygous diploids.) The absence of rpL33A in the Δ*A* mutant and the attendant reduction in 40S-subunit levels also reduce the rate of subunit joining, but in this case there is no competition for the functional subunits.

We found that overexpressing $tRNA_i^{Met}$, alone or together with eIF2 (TC), partially suppresses the Gcd$^-$ phenotype of the *rpl33a-G76R* mutation. Such suppression also occurs with *gcd* mutations in subunits of eIF2 or eIF2B that derepress *GCN4* by reducing TC formation (38). This has likewise been observed for mutations in initiation factors that impair the rate of TC recruitment, e.g., eIF1A (21). All of the latter mutations are thought to produce Gcd$^-$ phenotypes by reducing the rate of TC recruitment to 40S subunits scanning the *GCN4* mRNA leader after they complete the translation of uORF1, increasing the proportion of 40S subunits that reach uORF4 without rebinding the TC and, consequently, bypassing uORF4 and reinitiating downstream at *GCN4* instead. Boosting TC levels in these mutants restores efficient reinitiation at uORF2 to -4 and thereby prevents reinitiation at *GCN4* (38).

It is unlikely that the *rpl33a-G76R* or Δ*A* mutations derepress *GCN4* translation by a mechanism involving impaired TC loading. First, the mutations affect the 60S subunit, which should not be present during the process of scanning from uORF1 to uORF4. Second, the mutations derepress *GCN4-lacZ* fusions containing either all four uORFs or uORF4 alone by similar degrees. Gcd$^-$ mutations that impair TC assembly or TC loading on 40S subunits have little effect on *GCN4* expression in the presence of uORF4 alone, because their effects on TC recruitment are greatly magnified by the reinitiation process that occurs after uORF1 translation (38). Because the *rpl33a* mutations clearly affect 40S- to 60S-sububnit joining, giving rise to abundant half-mer polysomes, the simplest interpretation of their Gcd$^-$ phenotypes is that they allow 40S subunits that reach uORF4 as fully assembled PICs (i.e., containing the TC) to bypass uORF4 because of a defect in subunit joining. The delay in subunit joining could allow a fraction of these PICs to abort reinititation at uORF4, resume scanning, and reinitiate further downstream at *GCN4*. This aberrant form of leaky scanning would also occur at the elongated version of uORF1, which cannot support reinitiation at *GCN4*, explaining why *rpl33a-G76R* decreases the inhibitory effect of this element, as well as solitary uORF4, on *GCN4* translation.

One way to account for this aberrant leaky scanning is to propose that a defect in subunit joining at the uORF4 AUG codon increases the probability of dissociation of Met-$tRNA_i^{Met}$ from the P site of the 40S subunit, which then allows the resumption of scanning downstream to *GCN4*. This would occur following hydrolysis of GTP by the TC and the release of eIF2-GDP from the PIC. Increasing the concentration of Met-$tRNA_i^{Met}$ would decrease its rate of disassembly from the PIC by mass action, enabling the PIC to remain intact long enough for the subunit joining reaction (impaired by *rpl33a-G76R*) to occur at the uORF4 AUG codon. Whereas overexpressing $tRNA_i^{Met}$ could prevent Met-$tRNA_i^{Met}$ loss at uORF4 (and thus reverse the Gcd$^-$ phenotype), it would not correct the low rate of subunit joining conferred by *rpl33a-G76R* and Δ*A*. Furthermore, overexpressing Met-$tRNA_i^{Met}$ should not suppress the ribosome biogenesis defects of these mutants. The last stipulations of our model can explain why overexpressing Met-$tRNA_i^{Met}$ fails to suppress the Slg$^-$ phenotypes of the *rpl33a* mutants.

It is noteworthy that Δ*A* differs from *rpl33a-G76R* in preventing full derepression of *HIS4-lacZ* expression in *GCN2 GCN3* cells under amino acid starvation conditions (last two lines of Table 3). In this respect, Δ*A* resembles the Δ*rpl16b* mutation described previously (23) in conferring moderate Gcd$^-$ and Gcn$^-$ phenotypes. We have proposed that the Gcn$^-$ phenotype of the Δ*rpl16b* mutation results from leaky scanning of the *GCN4* AUG codon under starvation conditions, whereas leaky scanning of uORF4 elicits the Gcd$^-$ phenotype of this mutation under nonstarvation conditions (23). Leaky scanning of uORF1 could also contribute to the Gcn$^-$ phenotype because translation of uORF1 is required for reinitiation at *GCN4* under starvation conditions. To explain why *rpl33a-G76R* produces only a strong Gcd$^-$ phenotype, we suggest that its more severe subunit joining defect than that of Δ*A* or Δ*rpl16b* results in such a high level of leaky scanning at uORF2 to -4 that these defects overpower the opposing effects of leaky scanning at uORF1 and *GCN4*, to yield a net derepression of *GCN4* translation (and *HIS4-lacZ* expression) that is comparable to the WT-induced level.

It is interesting that the Slg$^-$ phenotypes of *rpl33a-G76R* and Δ*A* mutants are partially suppressed by overexpression of PAB1. Because PAB1 has been implicated in 60S-subunit joining in yeast (61), we considered the possibility that its overexpression corrects the defect in subunit joining imposed by *rpl33a-G76R* and Δ*A*. However, this possibility is at odds with the fact that the hc*PAB1* plasmid does not significantly diminish half-mer formation in *rpl33a-G76R* cells, nor does it suppress the Gcd$^-$ phenotypes of either *rpl33a* mutant. The hc*PAB1* plasmid also does not reduce the Slg$^-$ or Gcn$^-$ phenotypes of a deletion of the gene encoding the subunit joining factor eIF5B (Δ*fun12*) (data not shown). Thus, we conclude that PAB1 overexpression does not rescue defective subunit joining. Interestingly, the hc*PAB1* plasmid substantially increased both 25S and 18S rRNA levels (see Fig. S1A and B in the supplemental material) without fully correcting the reduced 25S/18S rRNA ratio in *rpl33a-G76R* cells. Hence, we think that the hc*PAB1* plasmid suppresses the Slg$^-$ phenotype of *rpl33a-G76R* cells primarily by boosting ribosomal-subunit levels but without completely eliminating subunit imbalance. More work is required to determine whether PAB1 overexpression diminishes defects in subunit biogenesis when rpL33A is either mutated or completely absent or whether it stabilizes defective subunits in the *rpl33a-G76R* mutants.

It was shown previously that the hc*PAB1* plasmid is a dosage suppressor of the temperature-sensitivity phenotypes conferred by the *rpc31-236* and *rpc10-30* mutations in Pol III subunits that substantially reduce the steady-state levels of $tRNA_i^{Met}$ (57). However, we found that the hc*PAB1* plasmid did not suppress the growth defects of mutations in eIF2, eIF2B, or the m^1A58 methyltransferase for $tRNA_i^{Met}$. As noted above, the Slg^- and Gcd^- phenotypes of these mutants are suppressed by overexpressing $tRNA_i^{Met}$ (8; data not shown), consistent with their defects in $tRNA_i^{Met}$ synthesis or TC assembly. Thus, it is unclear whether suppression of the growth defects of *rpc31-236* and *rpc10-30* mutants by the hc*PAB1* plasmid involves ameliorating a defect in TC assembly.

The idea that the *rpl33a-G76R* mutation interferes with subunit joining is consistent with several indications that rpL33 is required for a correct interaction of the 60S subunit with the 40S subunit. Cross-linking data suggest that L35a, the rat homolog of yeast rpL33, is located near the A and P sites of the 60S subunit (68). Moreover, L35a binds in vitro to initiator tRNA and elongator tRNAs (69). Finally, rpL33 was found to interact with 60S protein rpL2A (26), which participates in a conserved protein-rRNA intersubunit bridge at the 40S-subunit–60S-subunit interface (63). The *rpl33a-G76R* mutation introduces an extra positively charged residue into the rigid loop that belongs to a putative RNA-binding domain in rpL33, and we found recently that replacement of Gly-76 with Lys or the nearby Gly-69 with Arg also yields strong Gcd^- phenotypes (unpublished observations). Hence, it is tempting to propose that these mutations lead to an inappropriate interaction of rpL33 with Met-$tRNA_i^{Met}$ in the P site or a segment of rRNA that somehow interferes with subunit joining.

Our findings indicate that rpL33 also plays an important role in ribosome biogenesis. Shifting the *rpl33a-G76R* mutant to 37°C leads to a progressive decrease in the ratio of the 60S subunit to the 40S subunit, indicating a relatively greater effect on 60S- versus 40S-subunit accumulation. This could result from impairment of 60S biogenesis, decreased stability of preexisting 60S subunits, or both. A defect in 60S subunit biogenesis is indicated by our Northern analysis of precursor and mature rRNAs after shifting the *rpl33a-G76R* mutant to 37°C. We observed an accumulation of the 35S precursor and a decrease in 27S and 20S pre-rRNAs, indicating a reduction in the rate of 35S cleavage at the A0, A1, and A2 sites in the 90S preribosomal particle that generates the pre-40S and pre-60S particles. There is also formation of aberrant <25S and 22.5S species that result from cleavage at the C2 or D processing sites in the absence of A0, A1, and A2 cleavage. Thus, the *rpl33a-G76R* mutation reduces the rate of processing events in the beginning of the pathway required for both 40S and 60S subunit biogenesis. Consistent with this, the amounts of mature 25S and 18S rRNA relative to total RNA decrease in the mutant at the restrictive temperature. The *rpl33a-G76R* mutation also increases the ratio of the 27SA2 precursor to mature 25S rRNA, suggesting an impairment of processing steps in the pre-60S particle. By contrast, the ratio of the 20S precursor to mature 18S rRNA is not elevated in the mutant, indicating efficient maturation and export of the 40S subunit.

Thus, our results strongly suggest that rpL33A is a component of pre-60S particles and contributes to one or more critical steps in the maturation of 60S subunits. Consistent with this idea, there is mass spectrometry data supporting the presence of rpL33 in early pre-60S particles (20, 51). Second, rpL33 has been shown to copurify with NOP7, a nucleolar protein essential for the processing and maturation of 27S pre-rRNA and for 60S subunit biogenesis (33). Third, we found that overexpression of WT rpL33A confers allele-specific suppression of mutations in *NOP7* and *DRS1*, encoding other nonribosomal components of pre-60S particles.

Considering that the mutation of *RPL33A* strongly impairs A0-A1-A2 processing, it could be proposed that rpL33 also resides in the 90S preribosome and directly influences these early processing events. However, it is important to note that the inhibition of late steps in the 60S pre-rRNA processing pathway seems to indirectly affect early steps in the processing of 35S pre-rRNA (73). Also, the possibility that processing defects could be secondary consequences of reduced translation of r-proteins or other ribosome biogenesis factors in the *rpl33* mutant backgrounds cannot be excluded. Consistent with the first idea, rpL33 was found in the 90S preribosome described in the 1970s (66) and was classified as an early assembled r-protein (41, 42). Moreover, recent mass spectrometry data revealed an association of rpL33 with PWP2, a conserved 90S preribosomal component essential for proper endonucleolytic cleavage of 35S rRNA at A0-A1-A2 (26). It should be noted, however, that other large preribosomal particles sedimenting at ~90S may correspond to the earliest pre-60S particles (67), including the highly complex nucleolar transitional pre-40S-60S particles (reviewed in reference 64). The NSA3-associating pre-rRNP complex (51) is an example of a highly complex nucleolar transitional pre-40S -60S particle, and rpL33 was found associated with NSA3/CIC1 (26). Nevertheless, whereas PWP2 is present in the earliest nucleolar pre-90S particle, it was not detected in the NSA3-associated pre-rRNP complex. Thus, the association with PWP2 favors the idea that rpL33 might reside in the classical 90S preribosome.

The pre-rRNA processing phenotypes of *rpl* mutants were not systematically investigated, as was recently done for *rps* mutants (22). Whereas the absence or functional inactivation of r-protein L5, L11, L25, L28, or L30 leads to an accumulation of 27S pre-rRNAs, we observed decreased steady-state levels of 27S and 20S pre-rRNAs, with little accumulation of 23S pre-RNA in *rpl33a-G76R* cells at 37°C. The delay in processing at A0-A3 leads to low levels of the 23S species, and subsequent cleavage at C2 or D produces <25S and 22.5S species in *rpl33a-G76R* cells. The <25S and 22.5S species were described previously (i.e., in references 9, 22, 40, and 52) but not observed in the *rpl* mutants analyzed so far. Hence, it appears that rpL33 makes a distinctive contribution to multiple pre-rRNA processing reactions.

ACKNOWLEDGMENTS

We thank Dionisio Martín-Zanca and Rosa Esteban for helpful suggestions regarding this work and Thomas Dever for critical reading of the manuscript. We also thank John L. Woolford for the *nop7* and *drs1* mutants and for the hc*NOP7* and hc*DRS1* plasmids, Alan Sachs for the hc*PAB1* plasmid, and Javier de las Rivas for help with the 3D model of rpL33.

P.M.-M. has been supported by fellowship AP2000-4183 granted by the Spanish Ministerio de Educación y Ciencia (MEC). M.T. was supported by MEC grants BMC 2001-1676 and PTR-1995-1010.

REFERENCES

1. **Adams, C. C., J. Jakovljevic, J. Roman, P. Harnpicharnchai, and J. L. Woolford, Jr.** 2002. *Saccharomyces cerevisiae* nucleolar protein Nop7p is necessary for biogenesis of 60S ribosomal subunits. RNA **8**:150–165.
2. **Anderson, J., L. Phan, R. Cuesta, B. A. Carlson, M. Pak, K. Asano, G. R. Bjork, M. Tamame, and A. G. Hinnebusch.** 1998. The essential Gcd10p-Gcd14p nuclear complex is required for 1-methyladenosine modification and maturation of initiator methionyl-tRNA. Genes Dev. **12:**3650–3662.
3. **Asano, K., L. Phan, J. Anderson, and A. G. Hinnebusch.** 1998. Complex formation by all five homologues of mammalian translation initiation factor 3 subunits from yeast *Saccharomyces cerevisiae*. J. Biol. Chem. **17:**18573–18585.
4. **Bassler, J., P. Grandi, O. Gadal, T. Lessmann, E. Petfalski, D. Tollervey, J. Lechner, and E. Hurt.** 2001. Identification of a 60S preribosomal particle that is closely linked to nuclear export. Mol. Cell **8:**517–529.
5. **Belk, J. P., F. He, and A. Jacobson.** 1999. Overexpression of truncated Nmd3p inhibits protein synthesis in yeast. RNA **5:**1055–1070.
6. **Bernstein, K. A., S. Granneman, A. V. Lee, S. Manickam, and S. J. Baserga.** 2006. Comprehensive mutational analysis of yeast DEXD/H box RNA helicases involved in large ribosomal subunit biogenesis. Mol. Cell. Biol. **26:**1195–1208.
7. **Burke, D., D. Dawson, and T. Stearns.** 2000. Assay of β-galactosidase in yeast, p. 125. *In* D. Burke, D. Dawson, and T. Stearns (ed.), Methods in yeast genetics. Cold Spring Harbor Laboratory Press, Cold Spring Harbor, NY.
8. **Calvo, O., R. Cuesta, J. Anderson, N. Gutierrez, M. T. García-Barrio, A. G. Hinnebusch, and M. Tamame.** 1999. GCD14p, a repressor of GCN4 translation, cooperates with Gcd10p and Lhp1p in the maturation of initiator methionyl-tRNA in *Saccharomyces cerevisiae*. Mol. Cell. Biol. **19:**4167–4181.
9. **Colley, A., J. D. Beggs, D. Tollervey, and D. L. Lafontaine.** 2000. Dhr1p, a putative DEAH-box RNA helicase, is associated with the box C+D snoRNP U3. Mol. Cell. Biol. **20:**7238–7246.
10. **Cuesta, R., A. G. Hinnebusch, and M. Tamame.** 1998. Identification of *GCD14* and *GCD15*, novel genes required for translational repression of *GCN4* mRNA in Saccharomyces cerevisiae. Genetics **148:**1007–1020.
11. **de la Cruz, J., D. Kressler, and P. Linder.** 2004. Ribosomal subunit assembly, p. 258–285. *In* M. O. J. Olson (ed.), The nucleolus. Kluwer Academic Publishers, New York, NY.
12. **Deshmukh, M., Y. F. Tsay, A. G. Paulovich, and J. L. Woolford, Jr.** 1993. Yeast ribosomal protein L1 is required for the stability of newly synthesized 5S rRNA and the assembly of 60S ribosomal subunits. Mol. Cell. Biol. **13**:2835–2845.
13. **Deutschbauer, A. M., D. F. Jaramillo, M. Proctor, J. Kumm, M. E. Hillenmeyer, R. W. Davis, C. Nislow, and G. Giaever.** 2005. Mechanisms of haploinsufficiency revealed by genome-wide profiling in yeast. Genetics **169:**1915–1925.
14. **Dever, T. E., L. Feng, R. C. Wek, A. M. Cigan, T. F. Donahue, and A. G. Hinnebusch.** 1992. Phosphorylation of initiation factor 2α by protein kinase GCN2 mediates gene-specific translational control of *GCN4* in yeast. Cell **68:**585–596.
15. **Dever, T. E., W. Yang, S. Åström, A. S. Byström, and A. G. Hinnebusch.** 1995. Modulation of $tRNA_i^{Met}$, eIF-2, and eIF-2B expression shows that *GCN4* translation is inversely coupled to the level of eIF-2 · GTP · Met-$tRNA_i^{Met}$ ternary complexes. Mol. Cell. Biol. **15:**6351–6363.
16. **Dragon, F., J. E. Gallagher, P. A. Compagnone-Post, B. M. Mitchell, K. A. Porwancher, K. A. Wehner, S. Wormsley, R. E. Settlage, J. Shabanowitz, Y. Osheim, A. L. Beyer, D. F. Hunt, and S. J. Baserga.** 2002. A large nucleolar U3 ribonucleoprotein required for 18S ribosomal RNA biogenesis. Nature **417:**967–970.
17. **Dresios, J., I. L. Derkatch, S. W. Liebman, and D. Synetos.** 2000. Yeast ribosomal protein L24 affects the kinetics of protein synthesis and ribosomal protein L39 improves translational accuracy, while mutants lacking both remain viable. Biochemistry **39:**7236–7244.
18. **Dresios, J., P. Panopoulos, C. P. Frantziou, and D. Synetos.** 2001. Yeast ribosomal protein deletion mutants possess altered peptidyltransferase activity and different sensitivity to cycloheximide. Biochemistry **40:**8101–8108.
19. **Dresios, J., P. Panopoulos, K. Suzuki, and D. Synetos.** 2003. A dispensable yeast ribosomal protein optimizes peptidyltransferase activity and affects translocation. J. Biol. Chem. **278:**3314–3322.
20. **Fatica, A., A. D. Cronshaw, M. Dlakic, and D. Tollervey.** 2002. Ssf1p prevents premature processing of an early pre-60S ribosomal particle. Mol. Cell **9:**341–351.
21. **Fekete, C. A., D. J. Applefield, S. A. Blakely, N. Shirokikh, T. Pestova, J. R. Lorsch, and A. G. Hinnebusch.** 2005. The eIF1A C-terminal domain promotes initiation complex assembly, scanning and AUG selection in vivo. EMBO J. **24:**3588–3601.
22. **Ferreira-Cerca, S., G. Poll, P. E. Gleizes, H. Tschochner, and P. Milkereit.** 2005. Roles of eukaryotic ribosomal proteins in maturation and transport of pre-18S rRNA and ribosome function. Mol. Cell **20:**263–275.
23. **Foiani, M., A. M. Cigan, C. J. Paddon, S. Harashima, and A. G. Hinnebusch.** 1991. GCD2, a translational repressor of the *GCN4* gene, has a general function in the initiation of protein synthesis in *Saccharomyces cerevisiae*. Mol. Cell. Biol. **11:**3203–3216.
24. **Gallagher, J. E., D. A. Dunbar, S. Granneman, B. M. Mitchell, Y. Osheim, A. L. Beyer, and S. J. Baserga.** 2004. RNA polymerase I transcription and pre-rRNA processing are linked by specific SSU processome components. Genes Dev. **18:**2506–2517.
25. **Gavin, A. C., M. Bosche, R. Krause, P. Grandi, M. Marzioch, A. Bauer, J. Schultz, J. M. Rick, A. M. Michon, C. M. Cruciat, M. Remor, C. Hofert, M. Schelder, M. Brajenovic, H. Ruffner, A. Merino, K. Klein, M. Hudak, D. Dickson, T. Rudi, V. Gnau, A. Bauch, S. Bastuck, B. Huhse, C. Leutwein, M. A. Heurtier, R. R. Copley, A. Edelmann, E. Querfurth, V. Rybin, G. Drewes, M. Raida, T. Bouwmeester, P. Bork, B. Seraphin, B. Kuster, G. Neubauer, and G. Superti-Furga.** 2002. Functional organization of the yeast proteome by systematic analysis of protein complexes. Nature **415:**141–147.
26. **Gavin, A. C., P. Aloy, P. Grandi, R. Krause, M. Boesche, M. Marzioch, C. Rau, L. J. Jensen, S. Bastuck, B. Dumpelfeld, A. Edelmann, M. A. Heurtier, V. Hoffman, C. Hoefert, K. Klein, M. Hudak, A. M. Michon, M. Schelder, M. Schirle, M. Remor, T. Rudi, S. Hooper, A. Bauer, T. Bouwmeester, G. Casari, G. Drewes, G. Neubauer, J. M. Rick, B. Kuster, P. Bork, R. B. Russell, and G. Superti-Furga.** 2006. Proteome survey reveals modularity of the yeast cell machinery. Nature **440:**631–636.
27. **Grallath, S., J. P. Schwarz, U. M. Bottcher, A. Bracher, F. U. Hartl, and K. Siegers.** 2006. L25 functions as a conserved ribosomal docking site shared by nascent chain-associated complex and signal-recognition particle. EMBO Rep. **7:**78–84.
28. **Grandi, P., V. Rybin, J. Bassler, E. Petfalski, D. Strauss, M. Marzioch, T. Schafer, B. Kuster, H. Tschochner, D. Tollervey, A. C. Gavin, and E. Hurt.** 2002. 90S pre-ribosomes include the 35S pre-rRNA, the U3 snoRNP, and 40S subunit processing factors but predominantly lack 60S synthesis factors. Mol. Cell **10:**105–115.
29. **Granneman, S., and S. J. Baserga.** 2004. Ribosome biogenesis: of knobs and RNA processing. Exp. Cell Res. **296:**43–50.
30. **Granneman, S., M. R. Nandineni, and S. J. Baserga.** 2005. The putative NTPase Fap7 mediates cytoplasmic 20S pre-rRNA processing through a direct interaction with Rps14. Mol. Cell. Biol. **25:**10352–10364.
31. **Grant, C. M., P. F. Miller, and A. G. Hinnebusch.** 1994. Requirements for intercistronic distance and level of eIF-2 activity in reinitiation on *GCN4* mRNA vary with the downstream cistron. Mol. Cell. Biol. **14:**2616–2628.
32. **Harashima, S., and A. G. Hinnebusch.** 1986. Multiple *GCD* genes required for repression of GCN4, a transcriptional activator of amino acid biosynthetic genes in *Saccharomyces cerevisiae*. Mol. Cell. Biol. **6:**3990–3998.
33. **Harnpicharnchai, P., J. Jakovljevic, E. Horsey, T. Miles, J. Roman, M. Rout, D. Meagher, B. Imai, Y. Guo, C. J. Brame, J. Shabanowitz, D. F. Hunt, and J. L. Woolford, Jr.** 2001. Composition and functional characterization of yeast 66S ribosome assembly intermediates. Mol. Cell **8:**505–515.
34. **Helser, T. L., R. A. Baan, and A. E. Dahlberg.** 1981. Characterization of a 40S ribosomal subunit complex in polyribosomes of *Saccharomyces cerevisiae* treated with cycloheximide. Mol. Cell. Biol. **1:**51–57.
35. **Hinnebusch, A. G.** 1985. A hierarchy of *trans*-acting factors modulates translation of an activator of amino acid biosynthetic genes in *Saccharomyces cerevisiae*. Mol. Cell. Biol. **5:**2349–2360.
36. **Hinnebusch, A. G.** 1988. Mechanisms of gene regulation in the general control of amino acid biosynthesis in *Saccharomyces cerevisiae*. Microbiol. Rev. **52:**248–273.
37. **Hinnebusch, A. G.** 1997. Translational regulation of yeast *GCN4*. A window on factors that control initiator-tRNA binding to the ribosome. J. Biol. Chem. **272:**21661–21664.
38. **Hinnebusch, A. G.** 2005. Translational regulation of *GCN4* and the general amino acid control of yeast. Annu. Rev. Microbiol. **59:**407–450.
39. **Hinnebusch, A. G., and G. R. Fink.** 1983. Positive regulation in the general amino acid control of Saccharomyces cerevisiae. Proc. Natl. Acad. Sci. USA **80:**5374–5378.
40. **Kressler, D., J. de la Cruz, M. Rojo, and P. Linder.** 1998. Dbp6p is an essential putative ATP-dependent RNA helicase required for 60S-ribosomal-subunit assembly in *Saccharomyces cerevisiae*. Mol. Cell. Biol. **18:**1855–1865.
41. **Kressler, D., P. Linder, and J. de la Cruz.** 1999. Protein *trans*-acting factors involved in ribosome biogenesis in *Saccharomyces cerevisiae*. Mol. Cell. Biol. **19:**7897–7912.
42. **Kruiswijk, T., R. J. Planta, and J. M. Krop.** 1978. The course of the assembly of ribosomal subunits in yeast. Biochim. Biophys. Acta **517:**378–389.
43. **Lucchini, G., A. G. Hinnebusch, C. Chen, and G. R. Fink.** 1984. Positive regulatory interactions of the *HIS4* gene of *Saccharomyces cerevisiae*. Mol. Cell. Biol. **4:**1326–1333.
44. **Mager, W. H., R. J. Planta, J. P. G. Ballesta, J. C. Lee, K. Mizuta, K. Suzuki, J. R. Warner, and J. L. Woolford, Jr.** 1997. A new nomenclature for the cytoplasmic ribosomal proteins of Saccharomyces cerevisiae. Nucleic Acids Res. **25**:4872–4875.
45. **Meskauskas, A., and J. D. Dinman.** 2001. Ribosomal protein L5 helps anchor peptidyl-tRNA to the P-site in *Saccharomyces cerevisiae*. RNA **7:**1084–1096.
46. **Meskauskas, A., A. N. Petrov, and J. D. Dinman.** 2005. Identification of

functionally important amino acids of ribosomal protein L3 by saturation mutagenesis. Mol. Cell. Biol. **25:**10863–10874.
47. **Milkereit, P., H. Kuhn, N. Gas, and H. Tschochner.** 2003. The pre-ribosomal network. Nucleic Acids Res. **31:**799–804.
48. **Moritz, M., B. A. Pulaski, and J. L. Woolford, Jr.** 1991. Assembly of 60S ribosomal subunits is perturbed in temperature-sensitive yeast mutants defective in ribosomal protein L16. Mol. Cell. Biol. **11**:5681–5692.
49. **Müeller P. P., and A. G. Hinnebusch.** 1986. Multiple upstream AUG codons mediate translational control of *GCN4*. Cell **45**:201–207.
50. **Natarajan, K., M. R. Meyer, B. M. Jackson, D. Slade, C. Roberts, A. G. Hinnebusch, and M. J. Marton.** 2001. Transcriptional profiling shows that Gcn4p is a master regulator of gene expression during amino acid starvation in yeast. Mol. Cell. Biol. **21:**4347–4368.
51. **Nissan, T. A., J. Bassler, E. Petfalski, D. Tollervey, and E. Hurt.** 2002. 60S pre-ribosome formation viewed from assembly in the nucleolus until export to the cytoplasm. EMBO J. **21:**5539–5547.
52. **Oeffinger, M., A. Fatica, M. P. Rout, and D. Tollervey.** 2007. Yeast Rrp14p is required for ribosomal subunit synthesis and for correct positioning of the mitotic spindle during mitosis. Nucleic Acids Res. **35:**1354–1366.
53. **Raué, H. A.** 2004. Pre-ribosomal RNA processing and assembly in *Saccharomyces cerevisiae*: the machine that makes the machine, p. 199–222. *In* M. O. J. Olson (ed.), The nucleolus. Kluwer Academic Publishers, New York, NY.
54. **Ripmaster, T. L., G. P. Vaughn, and J. L. Woolford, Jr.** 1992. A putative ATP-dependent RNA helicase involved in *Saccharomyces cerevisiae* ribosome assembly. Proc. Natl. Acad. Sci. USA **89**:11131–11135.
55. **Rose, M. D., P. Novick, J. H. Thomas, D. Botstein, and G. R. Fink.** 1987. A *Saccharomyces cerevisiae* genomic plasmid bank based on a centromere-containing shuttle vector. Gene **60:**237–243.
56. **Rotenberg, M. O., M. Moritz, and J. L. Woolford, Jr.** 1988. Depletion of *Saccharomyces cerevisiae* ribosomal protein L16 causes a decrease in 60S ribosomal subunits and formation of half-mer polyribosomes. Genes Dev. **2**:160–172.
57. **Rubbi, L., S. Labarre-Mariotte, S. Chedin, and P. Thuriaux.** 1999. Functional characterization of ABC10α, an essential polypeptide shared by all three forms of eukaryotic DNA-dependent RNA polymerases. J. Biol. Chem. **27:**31485–31492.
58. **Saveanu, C., D. Bienvenu, A. Namane, P. E. Gleizes, N. Gas, A. Jacquier, and M. Fromont-Racine.** 2001. Nog2p, a putative GTPase associated with pre-60S subunits and required for late 60S maturation steps. EMBO J. **20:**6475–6484.
59. **Schäfer, T., D. Strauss, E. Petfalski, D. Tollervey, and E. Hurt.** 2003. The path from nucleolar 90S to cytoplasmic 40S pre-ribosomes. EMBO J. **22:** 1370–1380.
60. **Schmitt, M. E., T. A. Brown, and B. L. Trumpower.** 1990. A rapid and simple method for preparation of RNA from *Saccharomyces cerevisiae*. Nucleic Acids Res. **18:**3091–3092.
61. **Searfoss, A., T. E. Dever, and R. Wickner.** 2001. Linking the 3′ poly(A) tail to the subunit-joining step of the translation initiation: relations of Pab1p, eukaryotic translation initiation factor 5B (Fun12p), and Ski2p-Slh1p. Mol. Cell. Biol. **21:**4900–4908.
62. **Snyder, D. A., et al.** March 2004 posting date. Solution structure of the 50S ribosomal protein L35Ae from *Pyrococcus furiosus*. Northeast Structural Genomics Consortium target PfR48. http://www.rcsb.org/pdb.
63. **Spahn, C. M., R. Beckmann, N. Eswar, P. A. Penczek, A. Sali, G. Blobel, and J. Frank.** 2001. Structure of the 80S ribosome from *Saccharomyces cerevisiae*-tRNA-ribosome and subunit-subunit interactions. Cell **107:**373–386.
64. **Takahashi, N., M. Yanagida, S. Fujiyama, T. Hayano, and T. Isobe.** 2003. Proteomic snapshot analyses of preribosomal ribonucleoprotein complexes formed at various stages of ribosome biogenesis in yeast and mammalian cells. Mass Spectrom. Rev. **22:**287–317.
65. **Tornow, J., and G. M. Santangelo.** 1994. *Saccharomyces cerevisiae* ribosomal protein L37 is encoded by duplicate genes that are differentially expressed. Curr. Genet. **25:**480–487.
66. **Trapman, J., J. Retèl, and R. J. Planta.** 1975. Ribosomal precursor particles from yeast. Exp. Cell Res. **90:**95–104.
67. **Tschochner, H., and E. Hurt.** 2003. Pre-ribosomes on the road from the nucleolus to the cytoplasm. Trends Cell Biol. **13:**255–263.
68. **Uchiumi, T., M. Kikuchi, K. Terao, and K. Ogata.** 1985. Cross-linking study on protein topography of rat liver 60S ribosomal subunits with 2-iminothiolane. J. Biol. Chem. **260:**5675–5682.
69. **Ulbrich, N., E. Wool, P. Ackerman, and P. Sigler.** 1980. The identification by affinity chromatography of the rat liver ribosomal proteins that bind to elongator and initiator transfer ribonucleic acids. J. Biol. Chem. **255:**7010–7016.
70. **Underwood, M. R., and H. M. Fried.** 1990. Characterization of nuclear localizing sequences derived from yeast ribosomal protein L29. EMBO J. **9:**91–99.
71. **Valasek, L., A. A. Mathew, B. S. Shin, K. H. Nielsen, B. Szamecz, and A. G. Hinnebusch.** 2003. The yeast eIF3 subunits TIF32/α, NIP1/χ, and eIF5 make critical connections with the 40S ribosome in vivo. Genes Dev. **17:**786–799.
72. **van Beekvelt, C. A., M. de Graaff-Vincent, A. W. Faber, J. van't Riet, J. Venema, and H. A. Raué.** 2001. All three functional domains of the large ribosomal subunit protein L25 are required for both early and late pre-rRNA processing steps in *Saccharomyces cerevisiae*. Nucleic Acids Res. **29:**5001–5008.
73. **Venema, J., and D. Tollervey.** 1999. Ribosome synthesis in *Saccharomyces cerevisiae*. Annu. Rev. Genet. **33:**261–311.
74. **Vilardell, J., and J. R. Warner.** 1997. Ribosomal protein L32 of *Saccharomyces cerevisiae* influences both the splicing of its own transcript and the processing of rRNA. Mol. Cell. Biol. **17:**1959–1965.
75. **Wach, A.** 1996. PCR synthesis of marker cassettes with long-flanking homology regions for disruptions in *S. cerevisiae*. Yeast **12:**259–265.
76. **Wach, A., A. Brachat, R. Pöhlmann, and P. Philippsen.** 1994. New heterologous modules for classical or PCR-based gene disruptions in *Saccharomyces cerevisiae*. Yeast **10:**1793–1808.
77. **Warner, J. R., J. Vilardell, and J. H. Sohn.** 2001. Economics of ribosome biosynthesis. Cold Spring Harbor Symp. Quant. Biol. **66:**567–574.